Exploring mechanisms of compaction in salt-marsh sediments using Common Era relative sea-level reconstructions

 Matthew J. Brain[1*], Andrew C. Kemp[2], Andrea D. Hawkes[3], Simon E. Engelhart[4], Christopher H. Vane[5], Niamh Cahill[6], Troy D. Hill[7], Jeffrey P. Donnelly[8] and Benjamin P. Horton[9,10]

[1*]Department of Geography and Institute of Hazard. Risk and Resilience, Durham University, South Road, Durham, DH1 3LE, UK

[2]Department of Earth and Ocean Sciences, Tufts University, Medford, MA 02155, USA

[3]Department of Geography and Geology, University of North Carolina Wilmington, Wilmington, NC 28403, USA

[4]Department of Geosciences, University of Rhode Island, Kingston, RI 02881, USA

[5]Centre for Environmental Geochemistry, British Geological Survey, Keyworth, Nottingham, NG12 5GG, UK

[6]Department of Biostatistics and Epidemiology, School of Public Health, University of Massachusetts Amherst, Amherst, MA USA

[7] Yale School of Forestry and Environmental Studies, New Haven, CT 06511, USA

[8]Department of Geology and Geophysics, Woods Hole Oceanographic Institution, Woods Hole, MA 02543, USA

[9]Department of Coastal and Marine Science, Rutgers University, New Brunswick, NJ 08901, USA

[10]Division of Earth Sciences and Earth Observatory of Singapore, Nanyang Technological University, 639798, Singapore

* Corresponding author

Tel.: +44 191 334 3513

E-mail address: matthew.brain@durham.ac.uk

Abstract

Salt-marsh sediments provide precise and near-continuous reconstructions of Common Era relative sea level (RSL). However, organic and low-density salt-marsh sediments are prone to compaction processes that cause post-depositional distortion of the stratigraphic column used to reconstruct RSL. We compared two RSL reconstructions from East River Marsh (Connecticut, USA) to assess the contribution of mechanical compression and biodegradation to compaction of salt-marsh sediments and their subsequent influence on RSL reconstructions. The first, existing reconstruction ('trench') was produced from a continuous sequence of basal salt-marsh sediment and is unaffected by compaction. The second, new reconstruction is from a compaction-susceptible core taken at the same location. We highlight that sediment compaction is the only feasible mechanism for explaining the observed differences in RSL reconstructed from the trench and core. Both reconstructions display long-term RSL rise of ~1 mm/yr , followed by a ~19th Century acceleration to ~3 mm/yr. A statistically-significant difference between the records at ~1100 to 1800 CE could not be explained by a compression-only geotechnical model. We suggest that the warmer and drier conditions of the Medieval Climate Anomaly (MCA) resulted in an increase in sediment compressibility during this time period. We adapted the geotechnical model by reducing the compressive strength of MCA sediments to simulate this softening of sediments. 'Decompaction' of the core reconstruction with this modified model accounted for the difference between the two RSL reconstructions. Our results demonstrate that compression-only geotechnical models may be inadequate for estimating compaction and post-depositional lowering of susceptible organic salt-marsh sediments in some settings. This has important implications for our understanding of the drivers of sea-level change. Further, our results suggest that future climate changes may make salt marshes more susceptible to the impacts of RSL rise by enhancing sediment compressibility. We stress, however, that the cause of the softening remains enigmatic. Until this is better constrained, it is premature to widely extrapolate our findings to existing core-based reconstructions of Holocene RSL.

1. Introduction

Salt-marsh sediments are an important source of decadal- to centennial- and decimeter-scale relative sea-level (RSL) reconstructions spanning the past ~200 to 3000 years (Gehrels, 2000; Kemp et al., 2009). These reconstructions offer insight into the processes that cause sea-level change across a range of spatial and temporal scales (Gehrels et al., 2012; Kemp et al., 2015b; Saher et al., 2015) and constrain the relationship between sea level and climate (Kemp et al., 2011; Kopp et al., 2016). High salt-marsh environments that maintained their tidal elevation in response to RSL rise by primary productivity of *in situ* plant material and by trapping clastic sediment delivered by tides (Craft et al., 1993; Morris et al., 2002) are commonly targeted to produce RSL reconstructions using stratigraphically-ordered samples from a single core.

On the Atlantic coast of North America, high salt-marsh peat is waterlogged, highly organic and has low initial bulk densities, which render it prone to mechanical compression and mass loss and/or weakening by biodegradation (Bloom, 1964; Lillebø et al., 1999; van Asselen et al., 2009). These processes, together termed compaction (Allen, 2000), can reduce the vertical thickness of a stratigraphic column through time and cause post-depositional lowering (PDL) of core samples (Long et al., 2006). PDL results in an overestimate of the magnitude and rate of reconstructed RSL rise (Brain, 2015; Horton and Shennan, 2009). Quantifying the contribution of sediment compaction is therefore necessary to prevent misattribution of apparent RSL changes to climatic, cryospheric, oceanographic, geological, or tectonic forcing mechanisms (Dutton et al., 2015; Khan et al., 2015; Kopp et al., 2016; Rowley et al., 2013; Tamisiea, 2011).

To explore the causes of PDL in organic salt-marsh sediment and to investigate the utility of geotechnical models in estimating compaction, we compared two independent RSL reconstructions from the same location in East River Marsh, Connecticut, USA (Fig. 1). The compaction-free ('trench') RSL reconstruction was developed from a continuous sequence of basal salt-marsh sediment in contact with bedrock that did not experience PDL (Kemp et al., 2015b). We produced a new RSL reconstruction from a sediment core taken at the deepest point of the same trench, which comprises salt-marsh peats and muds that are susceptible to compaction. Due to their proximity, and in the absence of any obvious issues with the accuracy

and quality of our reconstructions, we assume that the most likely mechanism for observed differences between the trench and core RSL records is PDL caused by compaction. Our existing geotechnical model (Brain et al., 2011; Brain et al., 2012) underestimated compaction in the sediment core because its underlying conceptual framework only considers mechanical compression. We suggest that the climatic changes of the Medieval Climate Anomaly (MCA) resulted in a reduction in the compressive strength of organic salt-marsh sediment which caused PDL that is nearly an order of magnitude larger than through mechanical compression alone.
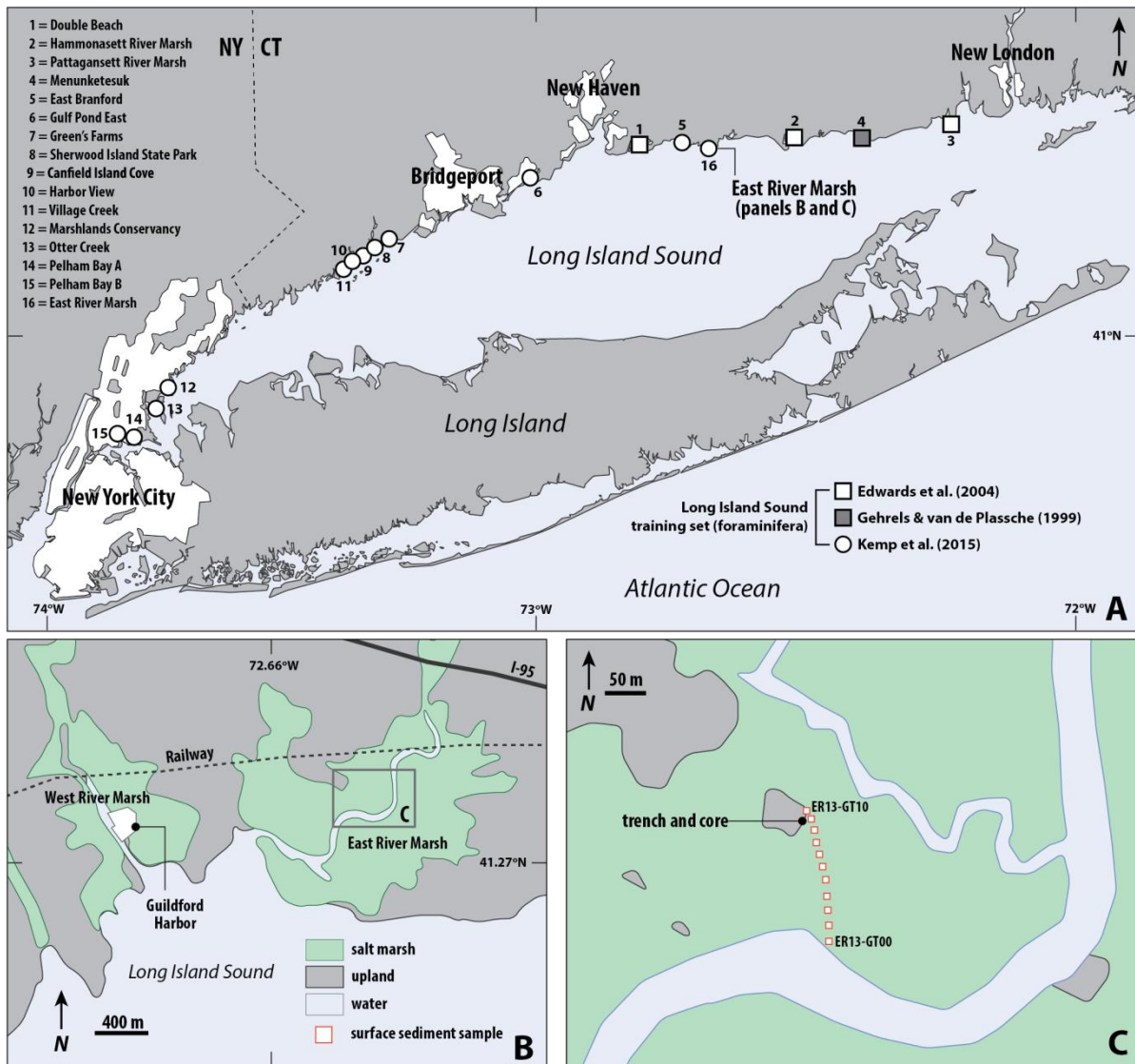
Figure 1. Location East River Marsh in Connecticut, USA. (A) The locations of 16 sites used to produce a regional-scale training set of modern foraminifera. (B, C) Locations of trench, core and surface sediment samples collected to characterize the geotechnical properties of modern salt-marsh sediment at East River Marsh. Modified from Kemp et al. (2015a).

2. Study area

East River Marsh is located on the Long Island Sound coast of Connecticut, USA (Fig. 1). Mean annual precipitation in this area is ~1270 mm and mean annual temperature is ~12˚C (PRISM, 2004). Great diurnal tidal range (mean lower low water, MLLW to mean higher high water, MHHW) at East River Marsh is 1.73 m. The modern salt marsh is comprised of three vegetation zones that are typical of salt marshes along the northeastern U.S. Atlantic coast (Niering and Warren, 1980; Orson et al., 1987; Redfield, 1972). Between mean tide level (MTL) and mean high water (MHW) is a narrow zone of *Spartina alterniflora* (tall form). The sediment deposited in this zone is grey-brown, organic mud in which marsh fiddler crabs (*Uca pugnax*) (Bertness and Miller, 1984; Katz, 1980) and purple marsh crabs (*Sesarma reticulatum*) (Schultz et al., 2016) are common. The high salt-marsh platform from MHW to MHHW is a wide area vegetated by *Distichlis spicata*, *Spartina patens*, and *Spartina alterniflora* (short form). The sediment in this zone is comprised of brown salt-marsh peat that is cohesive due to the presence of dense root networks and is rarely bioturbated by crab activity. From MHHW to highest astronomical tide (HAT), the dominant plants are *Phragmites australis* and *Iva fructescens*. Sediment deposited in this zone is amorphous, black and organic.

3. Methods

3.1 Approach and assumptions

Kemp et al. (2015b) excavated a trench at East River Marsh to expose the salt-marsh sediment overlying the gently sloping bedrock (Figs. 1 and. 2). They used the basal sediment in the trench to reconstruct RSL and assumed that the record was free from the effects of compaction and, therefore, did not undergo PDL. We produced a new RSL reconstruction using a core collected at the deepest part of the trench (section 3.2). The specific stratigraphy of the core (section 4.1) suggests that it may be more susceptible to compaction by mechanical compression than an unbroken sequence of high salt-marsh peat (Brain et al., 2012; Horton and Shennan, 2009). For this reason, it is unlikely that this core would be selected to produce a near-continuous Common Era RSL reconstruction (Allen, 1999; Brain et al., 2012; Gehrels, 2000; Kemp et al., 2009). Despite this, the RSL reconstruction from the core provides an opportunity to assess the predictive capacity of the compression-only geotechnical model developed by Brain et al. (2015; 2011; 2012).

Since the trench and core records were collected from the same location (within <10 m of each other; Fig. 2), regional-scale processes such as glacio-isostatic adjustment (GIA) and ocean dynamics cannot explain any differences between them and local-scale processes other than compaction (e.g. tidal-range change) would have an identical effect on both RSL records. If the chronologies and reconstructed marsh surface elevations for both the core and trench are suitably robust, we contend that the most likely explanation for any difference is PDL of the core samples caused by sediment compaction. The observable difference between RSL reconstructed from the trench and core is termed PDL_{field}.

To quantify the relative contributions of mechanical compression and biodegradation to PDL_{field} we used the geotechnical model of Brain et al. (Brain et al., 2011; 2012; section 3.3). This empirical model estimates mechanical compression by establishing the relationship between organic content (loss on ignition; LOI) and sediment geotechnical properties using a modern training set. This approach allowed us to estimate the compression properties of individual layers

in the core from LOI measurements, which circumvents the difficulty of obtaining samples suitable for geotechnical testing from depth.

Application of the model to core sediments estimates the amount of PDL experienced by each sample that we term PDL_{model}. If PDL_{field} and PDL_{model} are the same (within error), then sediment compaction arises solely or primarily from mechanical compression. Any residual differences between PDL_{field} and PDL_{model} must result from processes not considered by the conceptual framework that underpins the Brain et al. (2011; 2012) model, namely biodegradation-induced weakening.
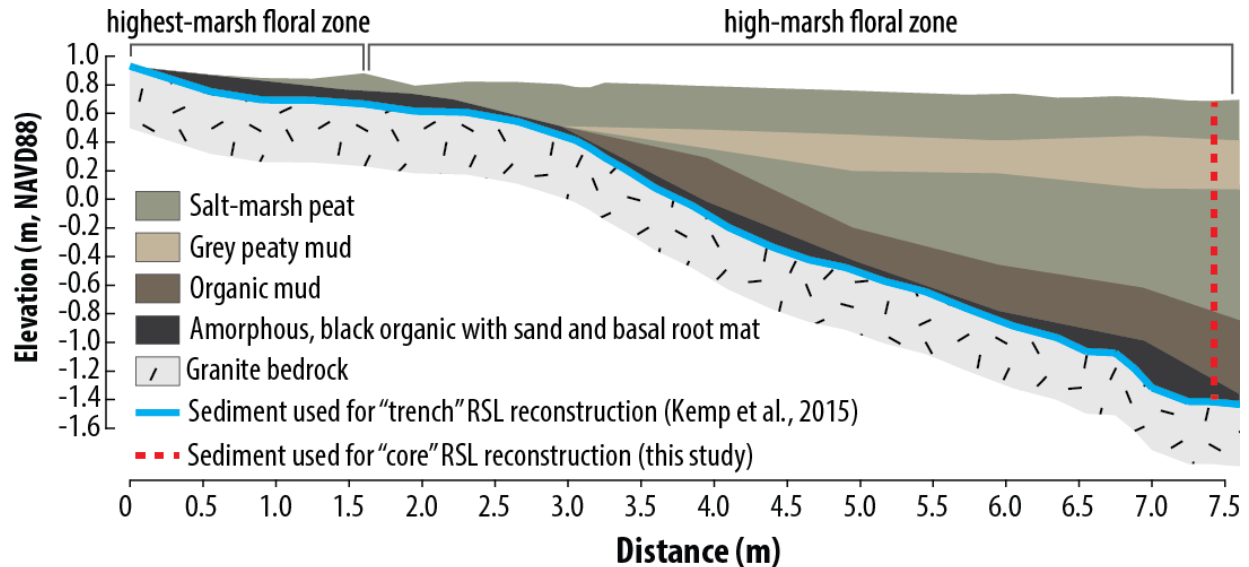
Figure 2. Cross section of sediment underlying East River Marsh described from a trench excavated along the underlying bedrock surface. Kemp et al. (2015a) produced a relative sea-level (RSL) reconstruction that was free from the influence of compaction using basal sediment from the trench (blue line). We produced a new RSL reconstruction from a sediment core collected at the deepest point of the trench (dashed red line) to investigate the role of compaction and the utility of a geotechnical model. The high-marsh floral zone is vegetated by *Spartina patens* and *Distichlis spicata*. The highest marsh floral zone is vegetated by *Phragmites australis* and *Iva fructescens*. Modified from Kemp et al. (2015a).

3.2 Reconstructing relative sea level

To ensure comparability between records, we reconstructed RSL from the core using the same methods and approaches that were previously employed to reconstruct RSL from the trench (see Kemp et al., 2015 for full details).

3.2.1 Reconstructing paleomarsh elevation

Salt-marsh foraminifera are sea-level indicators (proxies) because their vertical distribution is controlled by the frequency and duration of tidal flooding, which is primarily a function of tidal elevation (e.g. Horton and Edwards, 2006; Scott and Medioli, 1978). At 16 salt marshes on the north coast of Long Island Sound, the distribution of modern, intertidal foraminifera was described from a total of 254 surface sediment samples and paired elevation measurements (Fig. 1A; Edwards et al., 2004; Gehrels and van de Plassche, 1999; Kemp et al., 2015b; Wright et al., 2011). This regional-scale training set was used by Kemp et al. (2015) to develop a weighted-averaging (WA) transfer function for reconstructing paleomarsh elevation (PME), which is the tidal elevation at which an assemblage of foraminifera was formed. The WA transfer function was applied to assemblages of foraminifera enumerated in every other 1-cm thick sample from the East River Marsh core to reconstruct PME with sample-specific errors (~1σ) generated by bootstrapping (Juggins and Birks, 2012). Sample preparation and analysis (including taxonomy) followed the approach used to describe assemblages preserved in the trench samples (Kemp et al., 2015). To assess the ecological plausibility of each PME estimate, we measured the dissimilarity between core samples and their closest modern analogue in the regional training set using the Bray-Curtis distance metric (Jackson and Williams, 2004). If this minimum dissimilarity exceeded the 20th percentile of distances measured among all possible pairs of modern samples, the core sample was deemed to lack a modern analogue and we excluded it from the RSL reconstruction (Kemp et al., 2013; Simpson, 2012; Watcham et al., 2013). We used constrained hierarchical cluster analysis (CONISS) to identify distinctive, stratigraphically-ordered assemblages of foraminifera in the core (Grimm, 1987; Juggins, 2013). The number of groups was determined from a broken-stick plot.

3.2.2 Core chronology

The chronology of sediment accumulation in the core was established by radiocarbon dating of identifiable plant macrofossils found in growth position (Table 1), and by identification of historic pollution markers. To ensure comparability between records, we limited the use of pollution markers in the core to those previously identified and used in the trench record (Kemp et al., 2015). In addition, we ensured comparable coverage of radiocarbon dates between trench and core records. All dating results were combined to reconstruct the history of sediment accumulation in the core using Bchron (Haslett and Parnell, 2008; Parnell et al., 2008), which statistically models the relationship between dated samples and their depths in the core. This approach addresses issues associated with the merging of different chronological markers and techniques that vary in terms of precision, and where different techniques reveal variability in ages for similar depths (Sommerfield, 2006; Wright et al., 2017). Radiocarbon ages were calibrated as part of the Bchron routine using the IntCal13 calibration curve (Reimer et al., 2013) and pollution markers were treated as having a uniform age uncertainty. The age-depth model estimated the age of every 1-cm thick sample in the core with uncertainty that we present as a 95% credible interval. Further detail on the chronostratigraphic methods employed, and validation thereof using tide gauge records, is provided in Kemp et al. (2015).

Table 1. Reported radiocarbon ages for samples from the East River Marsh core.

Depth (cm)	ID	Age (^{14}C years)	Age Error (^{14}C years)	δ^{13}C (‰, VPDB)	Dated Material
58	OS-129653	180	20	-13.52	*Distichlis spicata* rhizome
75	OS-92676	385	25	-12.65	
87	OS-129654	500	20	-13.01	
98	OS-96813	590	30	-24.85	
98	OS-129651	680	20	-12.31	*Distichlis spicata* rhizome
104	OS-129652	880	25	-13.52	*Distichlis spicata* rhizome
109	OS-115115	915	20	-13.84	*Distichlis spicata* rhizome
121	OS-115116	1070	15	-14.95	*Distichlis spicata* rhizome
129	OS-92601	1130	25	-13.52	
141	OS-96814	1290	40	-14.08	
155	OS-92600	1540	25	-14.28	
167	OS-96815	1730	35	-14.45	
188	OS-92602	1840	25	-22.14	
204	OS-110630	1960	20	-15.02	*Distichlis spicata* rhizome

3.2.3 Rates of relative sea-level change

We reconstructed RSL by subtracting PME estimated by the WA transfer function (with uncertainty) from the measured elevation of each sediment sample. An age (with uncertainty) was assigned to each sample from the Bchron age-depth model. The individual data points in the resulting RSL reconstruction are unevenly distributed through time and are characterized by sample-specific age and vertical errors. To account for these characteristics in the core and trench reconstructions, we used the Error-in-Variables Gaussian Process (EIV-GP) model of Cahill et al. (2015a) to quantify RSL trends through time. We also used error-in-variables change-point regression (Cahill et al., 2015b; Carlin et al., 1992) to determine when the linear rate of RSL rise changed significantly. To permit the most direct comparison of the two RSL records we did not combine either reconstruction with tide-gauge data and did not detrend either dataset for the contribution from GIA. We quantified PDL_{field} using the EIV-GP models because the individual RSL data points do not have the same temporal distribution in each record.

3.3 Physical and geotechnical properties of salt-marsh sediment

3.3.1 Modern surface samples

To determine the geotechnical properties of modern salt-marsh sediments that are needed to empirically estimate terms in the compaction model (see Brain, 2015), we obtained 11 undisturbed surface sediment samples from East River Marsh (Fig. 1 C; Table 2). These modern samples capture the full elevation range of the contemporary salt marsh and the principal floral zones described previously (Table 2). We collected each sample by pushing a sampling ring (15 cm diameter, 15 cm depth) with a bevelled cutting edge into the surface sediment (Brain, 2015). To limit moisture loss prior to laboratory testing, each sediment sample was retained in the sampling ring and sealed using plastic wrap. The samples were stored in refrigerated conditions to limit bacterial decay.

Table 2. Description of modern surface samples collected from East River Marsh.

Sample ID	Summary description of vegetation assemblage
ERM13-GT00	Tall-form *Spartina alterniflora* (25% coverage). 75% of surface area is heavily-bioturbated mud.
ERM13-GT01	Short-form *Spartina alterniflora*.
ERM13-GT02	*Distichlis spicata*.
ERM13-GT03	*Distichlis spicata*, *Spartina patens* and short-form *Spartina alterniflora*
ERM13-GT04	*Distichlis spicata*, *Spartina patens* and short-form *Spartina alterniflora*
ERM13-GT05	*Distichlis spicata*, *Spartina patens* and short-form *Spartina alterniflora*
ERM13-GT06	*Distichlis spicata*, *Spartina patens* and short-form *Spartina alterniflora*
ERM13-GT07	*Distichlis spicata*, *Spartina patens* and short-form *Spartina alterniflora*
ERM13-GT08	*Phragmites australis Iva fructescens* and *Spartina patens*.
ERM13-GT09	*Phragmites australis Iva fructescens* and *Spartina patens*.
ERM13-GT10	*Toxicodendron radicans, Typha angustifolia, Spartina patens, Iva fructescens*

For each surface specimen, we measured LOI and bulk density using standard methods (Head, 2008; Head and Epps, 2011). LOI was determined by oven-drying (105°C for 24 h) and then subjecting samples to high (550°C for 4 h) ignition temperatures (Boyle, 2004; Head, 2008; Heiri et al., 2001; Plater et al., 2015). Presented LOI results are the mean and standard deviation of three determinations to assess variability in the small (2 g dry mass) sample masses analyzed (see Brain et al., 2015, for further justification on the use of LOI as a proxy measurement of organic content in decompaction modelling; see also Heiri et al., 2001). We measured particle density (specific gravity, G_s) using an automatic gas pycnometer. Presented results are the (unitless) mean of ten determinations. Standard deviation values were of the order ±0.001, and are not considered further. We calculated the voids ratio (e) from measured particle density data, sample dimensions and dry sample mass using the Height of Solids method (Head, 2008; Head and Epps, 2011).

We measured the compression behavior of the surface sediment samples using fixed-ring, front-loading oedometers, which subjected each sample (height = 19 mm; diameter = 75 mm) to one-dimensional (vertically loaded with zero lateral strain) compressive loading (Head and Epps, 2011). This method replicates the effects of loading by overburden sedimentation in the field, where lateral strain is prevented (Powrie, 2014). During the oedometer tests, load was incrementally added to each sample and maintained until primary consolidation ceased (i.e. when excess pore water pressures had dissipated and effective stress equaled total stress); we estimated this point for each loading stage using the vertical displacement versus square-root time method (Head and Epps, 2011).

We estimated values for the four parameters of the Brain et al. (2011; 2012) geotechnical model using the compression test data obtained for the modern samples: (1) the voids ratio at 1 kPa (e_1); (2) the recompression index (C_r, which describes the compressibility of the sample in its pre-yield, reduced compressibility state); (3) the compression index (C_c which describes sediment compressibility in its post-yield, increased compressibility state); and (4) the compressive yield stress (σ'_y, in kPa) that defines the transition from the reduced- to increased-compressibility condition. We estimated σ'_y by determining the effective stress value at which modelled recompression and compression lines intersect in plots of voids ratio against the common logarithm of vertical effective stress (i.e. $e\log_{10}\sigma'$ plots; Fig. 3 A). σ'_y, and hence the stress range (and so depth range) over which sediments experience reduced compressibility, is controlled by the nature of the sediment and its resistance to deformation resulting from, for example, desiccation (Hawkins, 1984), geochemical changes (Crooks, 1999; Greensmith and Tucker, 1971) or root shear strength (Gabet, 1998; Hales et al., 2009; Van Eerdt, 1985). This determines whether the sediment was previously exposed to a vertical effective stress greater than that resulting from the existing (in situ) overburden. Such sediments are referred to as overconsolidated and are denser and more resistant to compression than their normally-consolidated equivalents (Selby, 1993) in the pre-yield stress range (Fig. 3 A). A lower σ'_y therefore increases the compressibility of a sediment in response to a given vertical effective stress increase, permitting greater volume changes at lower values of vertical effective stress and, hence, at shallower depths (Fig. 3 B).

14
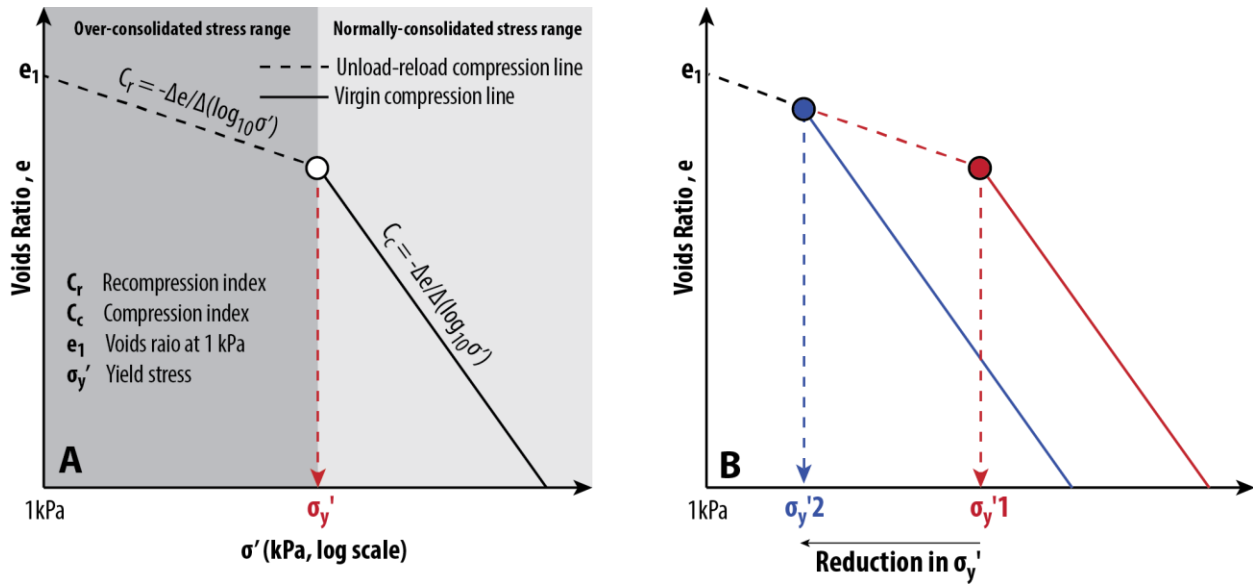
Figure 3. (A) Four-parameter model to describe compression behaviour in salt-marsh sediments. See text for further description. **(B)** The effect of reduced compressive yield stress, σ'_y, on the magnitude of volume change for a given change in effective stress. A reduction in yield stress from $\sigma'_y 1$ to $\sigma'_y 2$ causes a greater reduction in voids ratio (e, and, hence, volume) in response to a given vertical effective stress increase at effective stress values between $\sigma'_y 1$ to $\sigma'_y 2$.

3.3.2 Core samples

We collected the core using a Russian corer to minimize vertical mixing and compression of the sediment during sample recovery. Each core section was placed in a plastic sleeve and sealed with plastic wrap to prevent disturbance, desiccation and oxidation of the sediment. The core was stored at ~4°C to inhibit bacterial decomposition. We sliced the sediment core into contiguous, 2-cm thick samples and measured LOI and bulk density using one determination of each variable for each sample following standard methods (Head, 2008; Head and Epps, 2011). These measurements provide the input required to run the geotechnical model and subsequently estimate compaction and PDL_{model}.

In accordance with the methods outlined by Brain (2015), we estimated PDL_{model} using a numerical model (repeat-iteration, stochastic 'Monte Carlo', 5000 model runs), where each iteration simulated the compression behavior of the core from a set of feasible and locally-constrained physical and geotechnical properties. Uncertainty in PDL_{model} and predicted

15

bulk density was quantified from the mean and standard deviation of the suite of model runs. Within each of the 119, 2-cm thick layers and for each model run the physical and geotechnical properties are assumed uniform. Based on the downcore LOI profile (Fig. 4 A), we assigned an LOI value selected from a uniform probability distribution defined by a best estimate (equal to the measured value; Fig.4 A) and an error term of ± 1.4 percentage points (equal to half the range of the variability observed in the surface samples from East River Marsh).
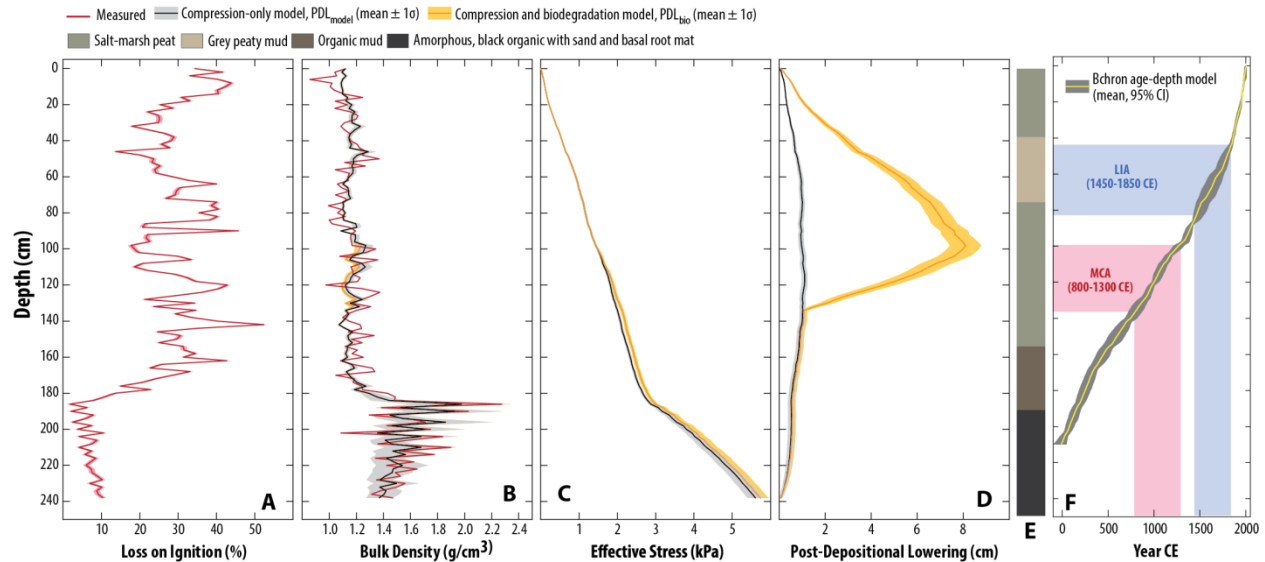
Figure 4. Physical and geotechnical properties, model results and stratigraphy of the East River Marsh core. (A) Measured downcore organic content. (B) Measured and modelled bulk density. (C) Modelled effective stress. (D) Model estimates of post-depositional lowering. (E) Lithostratigraphy. (F) Age–depth model (mean, with 95% credible interval, the timings of the Medieval Climate Anomaly (MCA; pink) and Little Ice Age (LIA; blue) are shown for reference and equated to depth intervals in the core. PDL_{model} (black/grey) refers to the geotechnical model in which compaction is caused only by mechanical compression. PDL_{bio} (orange/yellow) is the geotechnical model in which sediment deposited during the MCA was softened, see text for details.

16

4. Results

4.1 Site stratigraphy

The stratigraphy exposed in the East River Marsh trench is displayed in Fig. 2, and the specific stratigraphy of the core used to reconstruct RSL is presented in Fig. 4 E. Differences in the thickness of the black amorphous organic unit along the trench arise from small-scale variability in the topography of the bedrock surface. The granite bedrock is overlain by an amorphous black sandy organic unit at depths of 238-186 cm. In turn, this is overlain by units of organic mud (186-152 cm) and salt-marsh peat (152-0 cm), which has an elevated clastic content at 75-38 cm.

4.2 Relative sea level

4.2.1 Paleomarsh elevation

The lowest occurrence of foraminifera in the East River Marsh core was at a depth of 195 cm. Constrained cluster analysis of foraminiferal assemblages identified four distinct groups (Fig. 5 A). Below 80 cm (cluster four), *Jadammina macrescens* was the dominant species with the presence of *Trochammina inflata/Siphotrochammina lobata*, *Arenoparrella mexicana* and *Tiphotrocha comprimata*. Cluster three (80-58 cm) is characterized by *Jadammina macrescens* and a near absence of *Arenoparrella mexicana*. At 56-20 cm, cluster two was dominated by *Trochammina inflata*/*Siphotrochammina lobata*. The top 19 cm of the core included increased abundances of *A. mexicana* and *T. comprimata* (cluster one). These species were also the most common foraminifera present in the trench samples and in other cores from East River Marsh that were described by Nydick et al. (1995). In this study and that of Nydick et al. (1995), changes in foraminiferal assemblages do not correspond to visible changes in the clastic content of salt-marsh peat units. Application of the WA transfer function to the assemblages of foraminifera preserved in the core generated PME reconstructions (Fig. 5 C), which indicated that all samples in the core formed between MHW and HAT. High abundances of *J. macrescens* resulted in correspondingly higher PME reconstructions. This is consistent with the interpretation that the dominant species of foraminifera in the core are characteristic of high salt-marsh ecosystems on the United States and Canadian Atlantic coasts (e.g. Gehrels, 1994; Kemp

et al., 2012; Wright et al., 2011). The average, sample-specific uncertainty for PME reconstructions was ± 0.16 m (~± 10 % of the great diurnal tidal range).The measured dissimilarity between each core sample and its closest analogue in the modern training set was less than the 20th percentile of dissimilarity measured among all possible pairs of modern samples (Fig. 5 B). This result indicates that all core samples had an appropriate modern analogue and we therefore consider the results ecologically plausible.
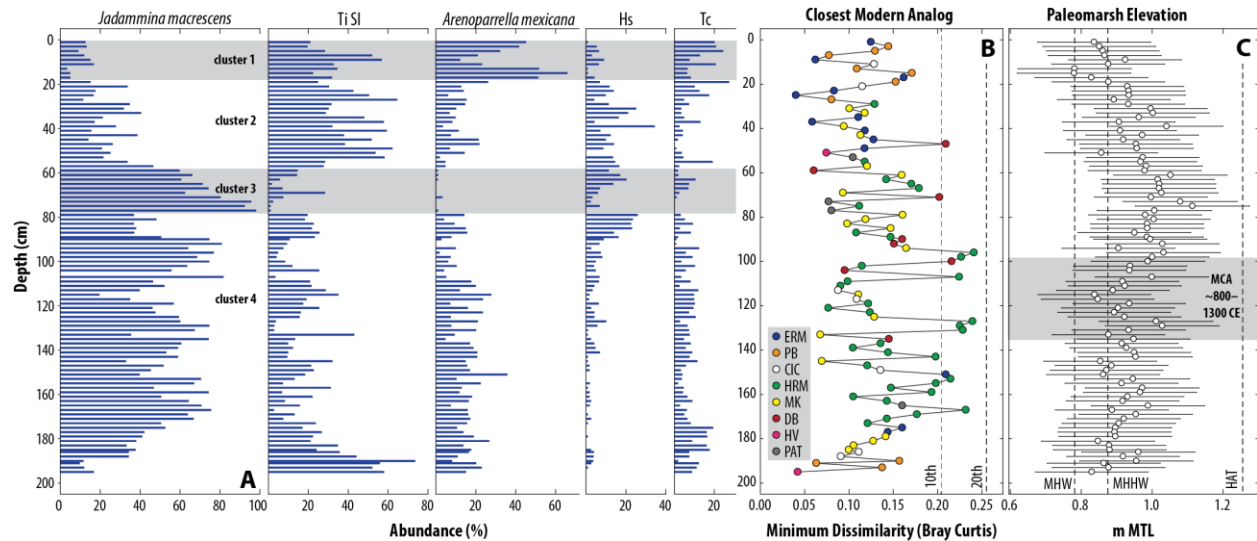
Figure 5. (A) Abundance of the five most common foraminifera in the East River Marsh core. Counts of *Trochammina inflata* and *Siphotrochammina lobata* (TiSl) were combined to ensure taxonomic consistency with previous studies that were part of the regional modern training set. Hs = *Haplophragmoides* spp., Tc = *Tiphotrocha comprimata*. Clusters 1-4 were identified using stratigraphically-constrained cluster analysis. (B) Dissimilarity between core samples and their closest modern analogue in the Long Island Sound training set measured using the Bray-Curtis metric. Symbols are colored by the eights sites that provided the closest modern analogue. The 20th percentile of dissimilarity among all pairs of modern samples (dashed vertical line) was used as a cut-off for determining which core samples had appropriate modern analogues. The 10th percentile is shown for comparison. ERM = East River Marsh, PB= Pelham Bay, CIC = Canfield Island Cove, HRM = Hammock River Marsh, MK = Menunketesuk, DB = Double Beach, HV = Harbor View, PAT = Pattagansett River Marsh. (C) Paleomarsh elevation (PME) reconstructed by applying the Long Island Sound weighted-averaging transfer function to assemblages of foraminifera preserved in the East River Marsh core. Sample-specific uncertainties were estimated by bootstrapping and constitute a ~1σ error. Dashed vertical lines show the elevation of mean high water (MHW), mean higher high water (MHHW) and highest astronomical tide (HAT).

4.2.2 Age-depth model

Interpretation of downcore trends in elemental and isotopic abundance followed the methods and rationale detailed in Kemp et al. (2015). The Bchron age-depth model predicted the age of every 1-cm thick interval of the core with an average uncertainty of ± 51 years (95% credible interval; Fig. 6). These results show that the ~2 m long core spans the period since ~0 CE and there is no indication of erosion or a hiatus in sedimentation, consistent with interpretations made in the field from the cross-section of sediment exposed in the trench. The rate of sediment accumulation was approximately linear at ~0.8 mm/yr from 0 CE (200 cm) to 1850 CE (~45 cm), when it increased to ~2.7 mm/yr.

4.2.3 Relative sea-level trends

The core reconstruction is comprised of 99 data points spanning ~100 to 2000 CE (Fig. 7 A). The trench reconstruction is comprised of 112 data points, covering the period ~200 BCE to 2000 CE (Fig. 7 B). Change-point regression (Fig. 8; Table 3) identified two successive linear RSL trends in both reconstructions. In the core, a statistically-significant increase in the rate of RSL rise from 0.72 mm/yr (95 % credible interval: 0.65 − 0.78 mm/yr) to 2.81 mm/yr (95 % credible interval: 1.98 − 4.06 mm/yr) occurred between 1671 and 1841 CE (95 % credible interval). In the trench, a statistically-significant increase in the rate of RSL rise from 0.92 mm/yr (95 % credible interval: 0.88 − 0.96 mm/yr) to 2.72 mm/yr (95 % credible interval: 1.64 − 4.50 mm/yr) occurred between 1739 and 1966 CE (95 % credible interval).

The EIV-GP model for the core indicates minor fluctuations in the rate of RSL rise around these persistent longer-term trends (Figs. 7 and 8). In the core, the rate of RSL rise decelerated to a minimum of 0.51 mm/yr (95 % credible interval: 0.17 − 0.86 mm/yr) in ~1300 CE, before accelerating to reach 2.91 mm/yr (95 % credible interval: 1.69 − 4.13 mm/yr;) in 2000 CE. In the trench reconstruction, the EIV-GP model shows that the rate of RSL rise peaked (1.08 mm/yr; 95 % credible interval: 0.77 − 1.39 mm/yr) at ~850 CE, then decelerated to a minimum (0.74 mm/yr; 95 % credible interval: 0.40 − 1.08 mm/yr) in ~1400 CE, before accelerating to a maximum of 2.1 mm/yr (95 % credible interval: 0.81 − 3.40 mm/yr) in 2000 CE (Fig. 8).

From ~1100 to 1800 CE, values of PDL_{field} indicate that the RSL reconstructions from the trench and the core described by the EIV-GP models do not overlap (Fig. 7 D), demonstrating a statistically-significant difference at core depths between ~47 and 111 cm. PDL_{field} decreases after ~1525 CE to zero by ~1950 CE.
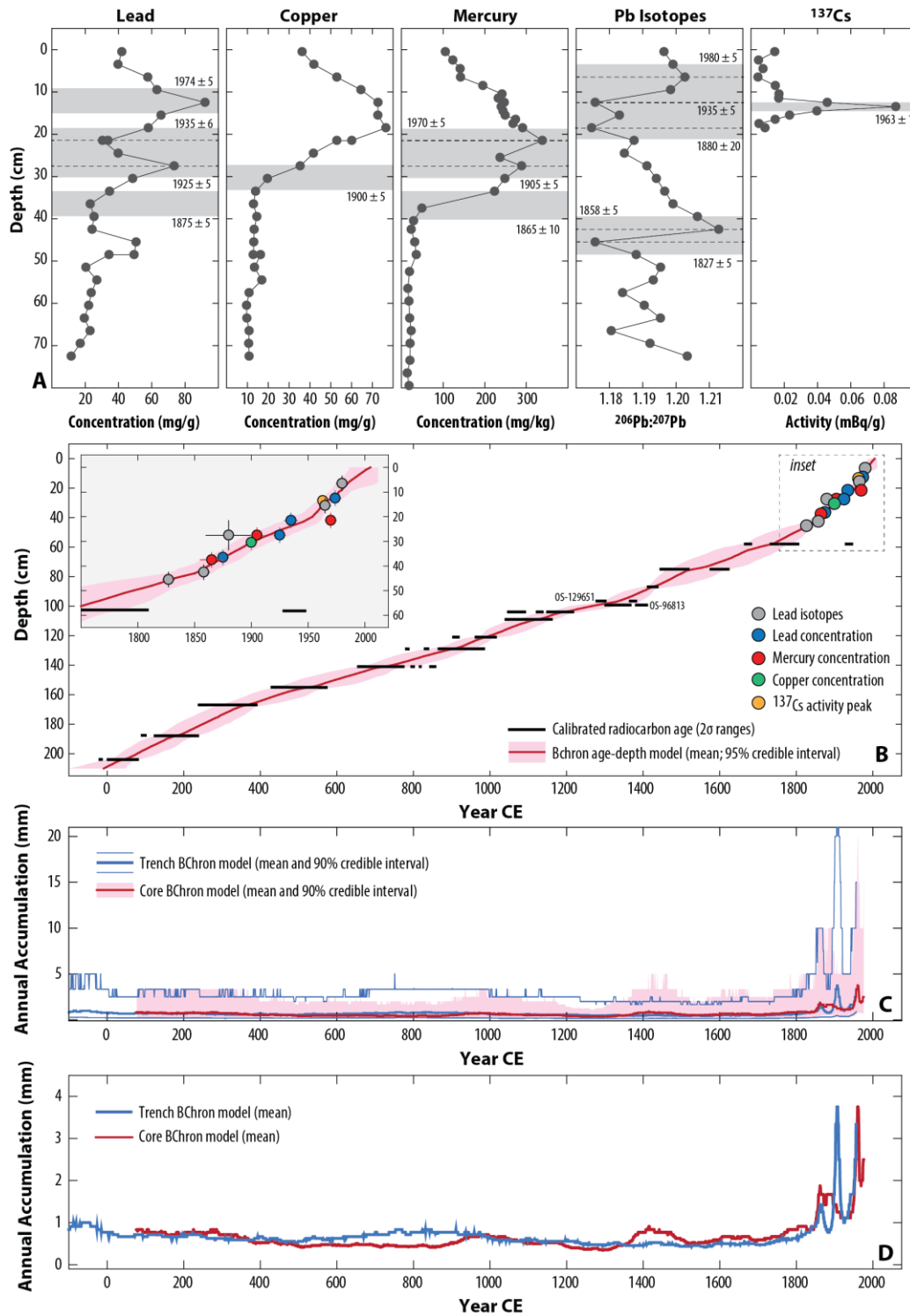
Figure 6. Chronology developed for the East River Marsh core. (A) Elemental and isotopic profiles used to recognize pollution markers of known age (listed on individual profiles). Grey bands represent the range of depths over which the horizon could occur. Dashed lines denote

21

mid-point of horizons that overlap. (B) Age-depth model developed for the core from radiocarbon dating (black bars representing 2σ possible calibrated age ranges) and pollution markers (colored circles). (C) Modelled annual accumulation curves for the trench and core records, with 90% credible intervals (CI). (D) Modelled mean annual accumulation curves for the trench and core records. For ease of comparison, age uncertainties are not shown.
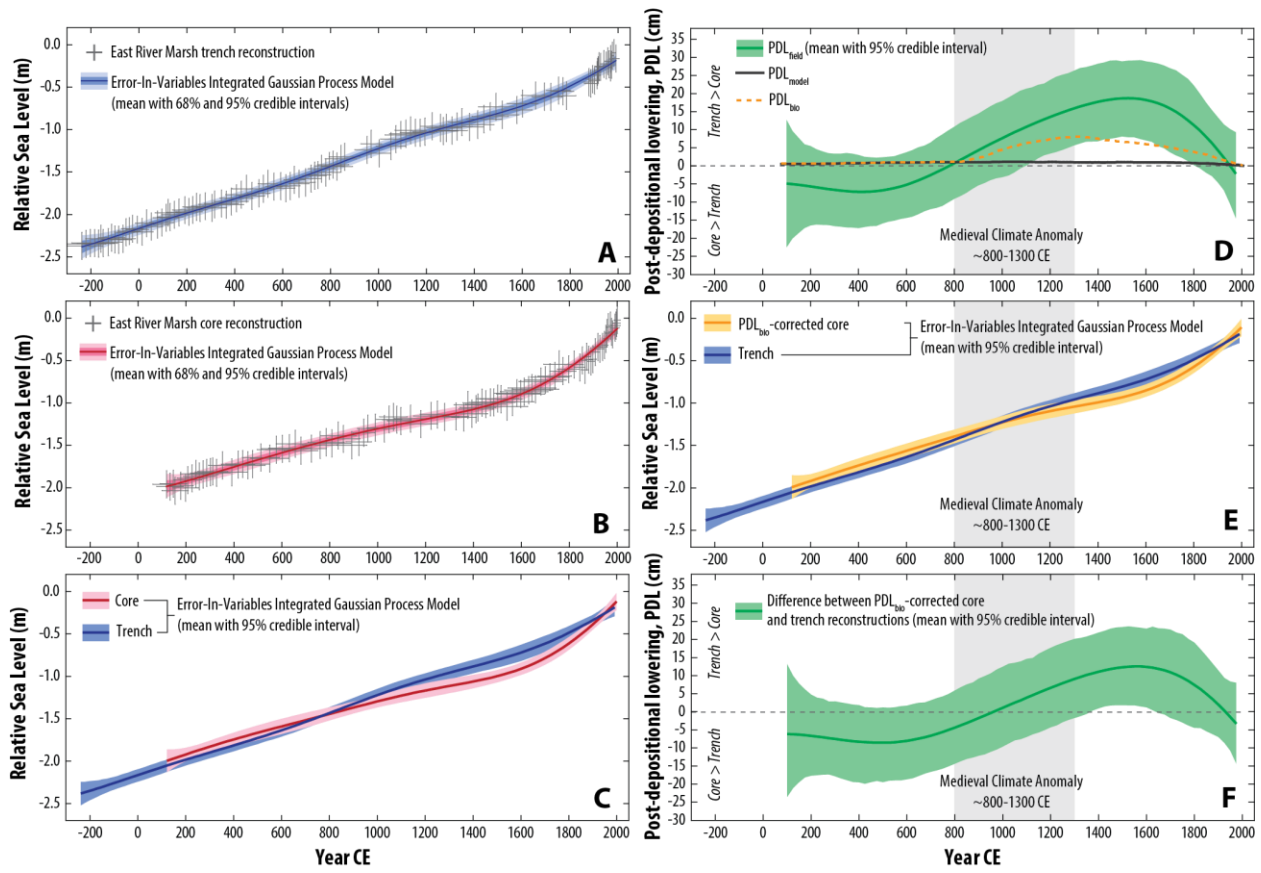
Figure 7. (A, B) Relative sea level reconstructed from the East River Marsh trench (Kemp et al., 2015) and core (this study). Grey crosses indicate the vertical and temporal uncertainty from the transfer function and age-depth model respectively. (C) Comparison of Errors-In-Variables Integrated Gaussian Process (EIV-IGP) models fitted to the trench and core relative sea-level reconstructions, with individual data points and uncertainties removed for clarity. **(D)** Observed difference between trench and core reconstructions (PDL$_{field}$; green) with predictions of post-depositional lowering from the compression-only model (PDL$_{model}$; black line) and the model that incorporated weakening of sediments deposited during the Medieval Climate Anomaly (PDL$_{bio}$; orange line). The grey box indicates the timing of the Medieval Climate Anomaly. (E) Comparison of EIV-IGP models fitted to the relative sea-level data from the trench and PDL$_{bio}$-corrected core reconstructions, with individual data points and uncertainties removed for clarity. (F) Modelled difference between trench and PDL$_{bio}$-corrected core RSL reconstructions.
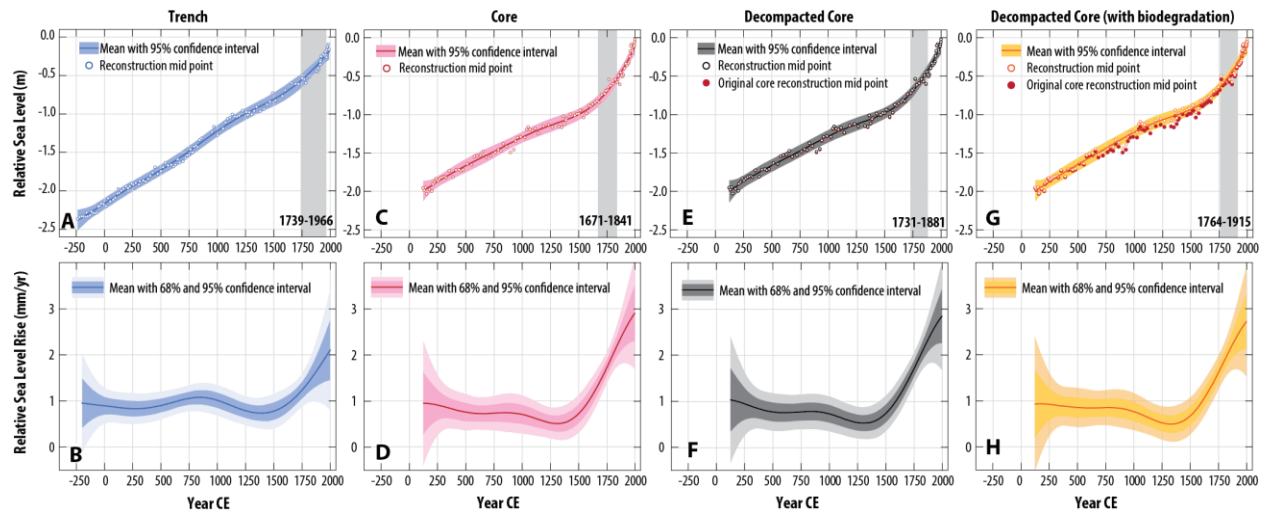
Figure 8. Top row: Comparison of Errors-In-Variables Integrated Gaussian Process (EIV-IGP) models fitted to the relative sea-level data from the East River Marsh trench, core and decompacted core reconstructions with individual reconstruction mid-points and, where appropriate, decompacted reconstruction mid-points. Vertical grey bars signify the timing (95% credible intervals) of the modelled changepoint, indicative of an acceleration in RSL. Bottom row: Rates of relative sea-level rise estimated by the EIV-IGP model for the East River Marsh trench, core and decompacted core reconstructions.

Table 3. Results of error-in-variables changepoint analysis undertaken on relative sea-level reconstructions considered in this study.

Reconstruction	Modelled changepoint (Year CE)		Pre-changepoint rate (mm/yr)		Post-changepoint rate (mm/yr)	
	Best estimate	95 % credible interval	Best estimate	95 % credible interval	Best estimate	95 % credible interval
Trench	1883	1739 - 1966	0.92	0.88 – 0.96	2.72	1.64 – 4.50
Core	1761	1671 – 1841	0.72	0.65 – 0.78	2.81	1.98 – 4.06
PDL$_{model}$-corrected core (compression only)	1815	1731 - 1881	0.75	0.68 – 0.82	3.46	2.27 – 5.19
PDL$_{bio}$-corrected core (compression and biodegradation)	1841	1764 - 1915	0.79	0.72 – 0.86	3.60	2.25 – 5.92

4.3 Physical and geotechnical properties of salt-marsh sediment

4.3.1 Modern surface sediment

The physical and geotechnical (compression) properties of the modern surface samples are displayed in Table 4. LOI values ranged from 9.12 % (ERM13-GT00) to 40.6 % (ERM13-GT10). Initial bulk density ranged from 0.99 g/cm^3 (ERM13-GT10) to 1.47 g/cm^3 (ERM13-GT00). Values of G_s ranged from 2.11 (ERM13-GT09) to 2.53 (ERM13-GT02). Values of initial (*in situ*) voids ratio, e, ranged between 2.38 (ERM13-GT00) and 8.84 (GR13-GT08).

In terms of compression properties, modern salt-marsh samples displayed e_1 values between 2.35 (ERM13-GT00) and 8.64 (GR13-GT08); C_r values between 0.02 (ERM13-GT00) and 0.15 (ERM13-GT09); C_c values between 0.63 (ERM13-GT00) and 4.12 (ERM13-GT08); and σ'_y, values between 3.5 kPa (ERM13-GT07) and 8.4 kPa (ERM13-GT08). The mean value of σ'_y was 5.1 kPa and the modal value was 4.0 kPa.

Table 4. Results of geotechnical tests performed on modern samples collected at East River Marsh. Loss on ignition results (mean and standard deviation, SD) are based on three determinations for each sample; standard deviations are expressed as percentage points.

Sample ID	Loss on ignition (%)		Particle density, G_s	Initial voids ratio, e_i	*In situ* bulk density (g/cm^3)	Voids ratio at 1 kPa, e_1	Recompression index, C_r	Compression index, C_c	Yield stress, σ'_y (kPa)
	Mean	SD							
ERM-13 GT00	9.12	0.82	2.45	2.38	1.47	2.35	0.02	0.63	4.00
ERM-13 GT01	10.17	0.21	2.50	2.52	1.43	2.47	0.03	0.65	6.00
ERM-13 GT02	13.45	0.76	2.53	3.88	1.28	3.77	0.06	1.02	4.75
ERM-13 GT03	16.28	0.85	2.40	3.76	1.31	3.72	0.02	1.17	4.00
ERM-13 GT04	21.64	2.85	2.32	6.08	1.14	6.03	0.03	1.45	4.00
ERM-13 GT05	16.17	1.67	2.40	5.61	1.21	5.51	0.07	2.00	7.50
ERM-13 GT06	34.29	2.06	2.29	7.80	1.13	7.62	0.12	2.63	5.00
ERM-13 GT07	26.38	2.31	2.26	7.25	1.12	7.23	0.11	2.58	3.50
ERM-13 GT08	34.02	1.35	2.16	8.84	1.07	8.64	0.14	4.12	8.40
ERM-13 GT09	29.42	0.84	2.11	7.50	0.99	7.27	0.15	2.91	5.00
ERM-13 GT10	40.63	2.40	2.27	7.60	1.03	7.43	0.12	2.73	4.00

4.3.2 Physical properties of core sediment

In the East River Marsh core (Fig. 4), LOI values varied from 1.76 % at 186 cm (amorphous black sandy organic unit) to 52.35 % at 142 cm (salt marsh peat). Within the amorphous black sandy organic unit (238-186 cm), mean LOI was 7.12 % (standard deviation, SD = 2.55 percentage points). The organic mud unit (186-152 cm) was characterized by mean LOI of 26.99 % (SD = 7.91 percentage points). The salt-marsh peat (152-0 cm) displayed a mean LOI value of 31.03 % (SD = 8.31 percentage points). Within this unit, the section with elevated clastic content (75-38 cm) displayed a mean LOI of 26.66 % (SD = 5.58 percentage points). As such, downcore patterns of LOI broadly corresponded with the visual stratigraphy observed, though we note intra-stratum variability.

Bulk density ranged from 0.86 g cm^{-3} (an unsaturated sample) at 6 cm (salt-marsh peat) to 2.27 g cm^{-3} at 186 cm in the amorphous black sandy organic unit. Mean bulk density in the amorphous black sandy organic unit (238-186 cm) was 1.56 g cm^{-3} (SD = 0.24 g cm^{-3}). Mean bulk density was 1.21 g cm^{-3} (SD = 0.09 g cm^{-3}) in the organic mud unit (186-152 cm). The salt-marsh peat (152- 0 cm) displayed a mean bulk density of 1.14 g cm^{-3} (SD = 0.10 g cm^{-3}).

5. Modelling compaction and post-depositional lowering

5.1 Model summary

Consistent with previous studies (Brain et al., 2015; 2012), we identified statistically-significant ($p \leq 0.001$), positive relationships between LOI and e_1, C_r, and C_c (Fig. 9). These relationships are physically, sedimentologically and ecologically plausible (Brain, 2015). More porous, low-density structures (i.e. higher voids ratios) occur in more organic sediments (i.e. greater LOI) that are created by vascular salt-marsh plants (DeLaune et al., 1994). These sediments are more prone to compression (i.e. greater values of C_r and C_c) than less organic deposits that are characterized by more compression-resistant sedimentary structures (Brain et al., 2011). G_s has a negative relationship with LOI (Fig. 9D) because organic matter is less dense than mineral material (Hobbs, 1986).

Yield stress (σ'_y) does not have a systematic relationship with LOI that can be obviously explained by ecological and sedimentological factors, or as a function of salt-marsh surface elevation (Table 4). This may result from waterlogged conditions near the salt-marsh surface that are persistent across the entire site and which limit desiccation. This prevents a large and highly-variable range of σ'_y from developing in the near-surface sediments (cf.Brain et al., 2012). The greater variability of σ'_y in samples ERM-13 GT01, ERM-13 GT05 and ERM-13 GT08 (Table 4) may reflect local differences in micro-topography at sampling locations and/or the differences in the geotechnical character of belowground biomass that affects confined compressive strength (Gabet, 1998; Van Eerdt, 1985).

From each modelled profile, we assigned values of e_1, C_r, C_c and G_s to each layer in the core based on their empirical relationship with measured LOI (Fig. 9; Table 5). We assigned values of σ'_y based on a continuous triangular probability distribution, defined by the modal value (4.0 kPa) and range (3.5-8.4 kPa) of σ'_y observed in surface sediments at East River Marsh (Table 4). We calculated *in situ* and depth-specific estimates of bulk density and effective stress by iteration, beginning with the surface layer and working downwards in each model run (Fig. 4 B and C). Linear regression of modelled and observed bulk density yielded a strong ($r^2_{adj} = 0.79$),

positive and statistically-significant (p <0.001) relationship (Figs. 4 B and 10 A). The estimated effective stress at the base of the core is 5.61 ± 0.21 kPa (Fig. 4 C). The modal value of σ'_y is exceeded at ~204 cm in the majority of model runs. Sediments below this depth are in their greater compressibility (normally consolidated) condition.

The decompaction routine is described in detail in Brain (2015). We estimated a peak PDL_{model} value of 1.11 ± 0.13 cm at 116 cm (Fig. 4 D), the approximate mid-point of the core. We note no obvious sharp inflections in the PDL_{model} curve.

5.2 Comparison of PDL$_{field}$ and PDL$_{model}$ and effect on the core RSL reconstruction

Between ~100 and 800 CE the trench and core RSL reconstructions overlap (Fig. 7 C), but PDL_{field} is negative and cannot be attributed to sediment compaction processes, which by definition can only decrease sediment thicknesses. Our compression model cannot predict negative values of PDL_{model} and during this interval PDL_{model} is positive, but generally < 1 cm (Fig. 7 D). We deem the compression model to be performing sufficiently robustly for sediments that formed during the time period between ~100 and 800 AD, since PDL_{model} values were modest. Between ~800 and 1950 CE, there is a systematic difference between PDL_{field} and PDL_{model}. While PDL_{model} remains positive and small (generally < 1 cm), PDL_{field} reaches ~19 cm (95 % CI: c. 7 – 29 cm), an order of magnitude greater. This demonstrates that our compression model is not performing with sufficient accuracy during this time period.

We decompacted the core using the PDL_{model} values, which generated a RSL record that is qualitatively and quantitatively indistinguishable from the original core reconstruction (Fig. 8) and the key differences between the core and trench reconstructions remain. As such, use of a compression-only geotechnical model to decompact cores of organic salt-marsh sediments still produces a RSL reconstruction that differs significantly from the 'true' (compaction-free) reconstruction recorded by the basal trench sediments.
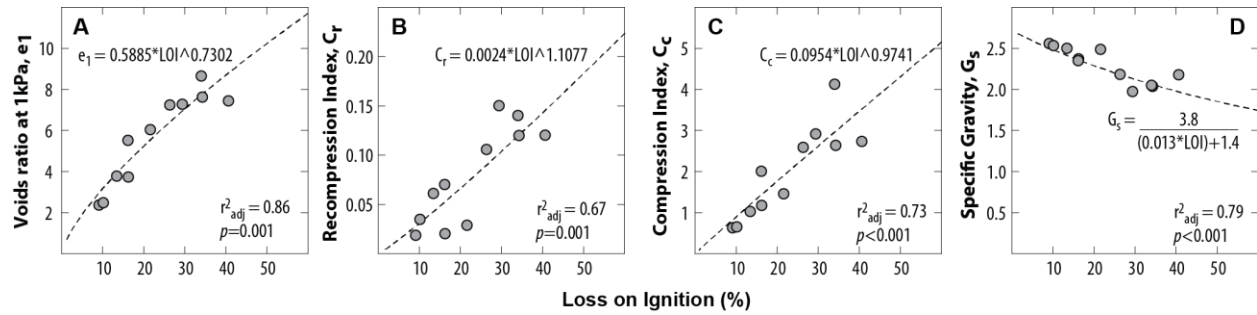
Figure 9. Observed relationships between geotechnical (A–C) and physical properties (D) of modern salt-marsh sediments collected from East River Marsh. For (D), the equation is from Hobbs (1986).

Table 5. Summary of error terms for regression equations used in decompaction modelling. All predicted variables are unitless.

Predicted (predictor) variable	Residuals passed Shapiro-Wilk normality test?	Regression model error distribution	± error term
G_s (loss-on-ignition)	No	Uniform	0.13
e_1 (loss-on-ignition)	Yes	Normal	0.84[*]
C_r (loss-on-ignition)	Yes	Normal	0.03[*]
C_c (loss-on-ignition)	Yes	Normal	0.58[*]

[*] error term is one standard error.
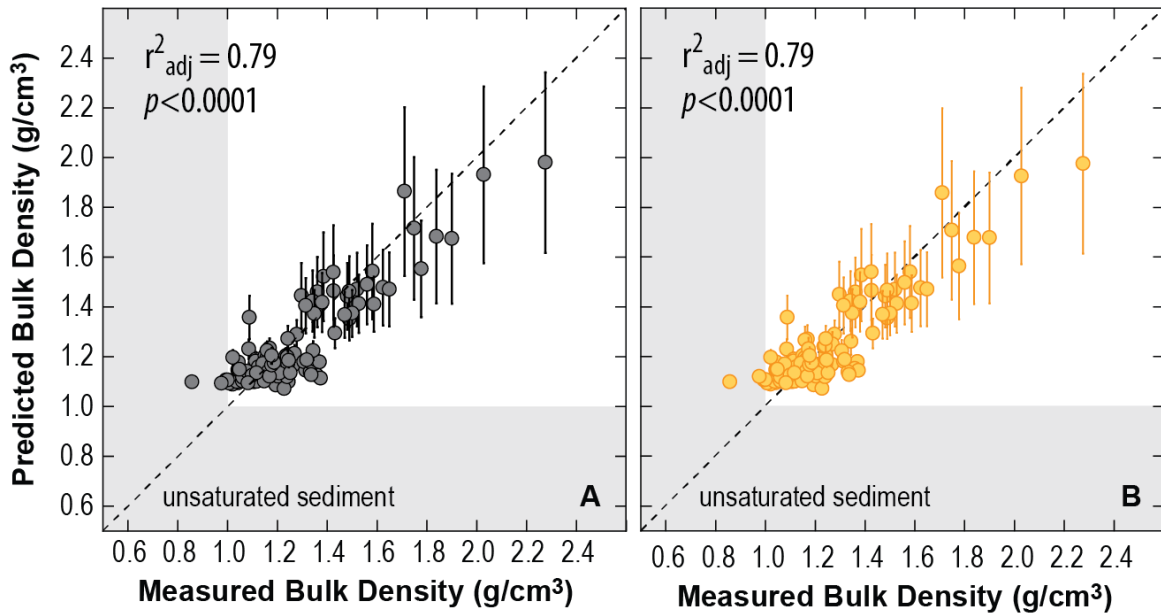
Figure 10. Model-predicted vs. measured bulk density for sediment samples in the East River Marsh core. (A) Results for the compression-only geotechnical model. (B) Results for the modified model, incorporating reduced yield stress values (weakening) for sediments that formed during the Medieval Climate Anomaly. See text for further details. Error bars for values of predicted bulk density represent the standard deviation of the mean of 5000 model runs.

6. Discussion

6.1 Age-depth and paleo-marsh elevation models

The statistically-significant differences in RSL between records between ~1100 and 1800 CE cannot be explained by our compression-only compaction model correction (PDL_{model}). It is important to determine the cause of the offset and whether it likely to affect similar high-resolution core-based records of Common Era RSL, because this has important implications for our understanding of the drivers of RSL and future projections thereof (Horton et al., 2014; Kopp et al., 2016). Similar high-resolution basal peat RSL records that span the Common Era are not ubiquitous and so cannot be used to effectively validate collocated core–based records.

32

We do not consider the differences between RSL records to be an artefact of the foraminifera-based transfer function estimates of PME obtained from the core and trench. We note some differences in reconstructed PME between records, but these are not sufficiently persistent to explain the entire offset between core and trench records (Fig. 11 A). Similarly, cluster analysis did not indicate any coincidence between any changes in core foraminiferal assemblages and the observed differences in reconstructed RSL between trench and core records (Fig. 5).
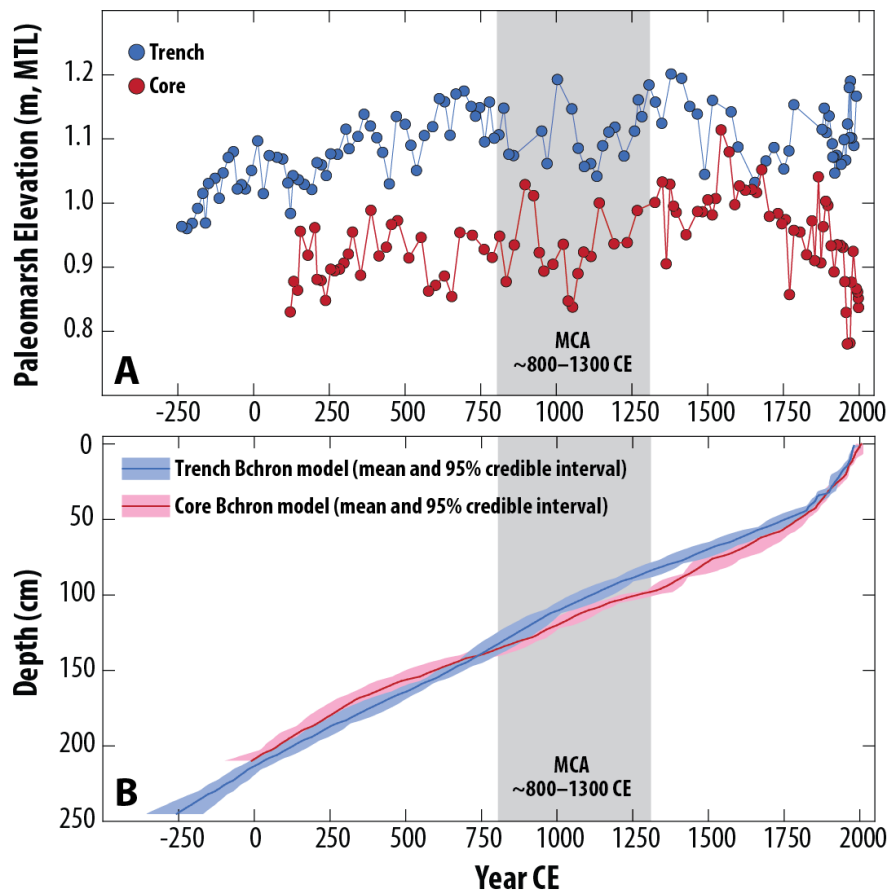
Figure 11. (A) Comparison of reconstructed paleomarsh elevations through time for the trench and core records. For clarity, only mid-points of estimates are shown. (B) Comparison of BChron age-depth models for the trench and core records.

The form of the modelled age-depth curve obtained from the core reconstruction, and how this differs from that obtained from that of the trench (Fig. 7; Fig.11 B), strongly resembles that of the RSL curve. This suggests that the RSL reconstruction is heavily driven by the age-depth model, rather than estimates of PME derived from the transfer function. The coverage and resolution of individual radiocarbon dates over the period of difference between records (~1100 – 1800 CE) is comparable between the trench and core reconstructions, such that the timing and form of is not heavily influenced by a single and/or erroneous date (Fig. 6). Similarly, the radiocarbon dates were obtained from rhizomes in *in situ* growth positions over the time period for which the difference between reconstructions is evident (Table 1; Kemp et al., 2015). On this basis, we consider the accuracy and quality of the age-depth model to be appropriately high for both core and trench reconstructions. In turn, we require an alternative explanation for the form of the age-depth curve, resultant RSL reconstruction and, ultimately, the differences observed between trench and core records.

6.2 Increased compressibility during the Medieval Climate Anomaly?

Given the close proximity of the locations from which the trench and core records were obtained at East River Marsh, the observed differences in reconstructed RSL cannot result from any drivers that would affect both records equally, including GIA, tidal range change and sediment supply. Having also eliminated reconstruction errors as the main cause of the observed differences, we argue that the only remaining explanation is sediment compaction and PDL of the core sediments. Since our compaction model does not account for the offset between records, it is possible that the underlying compression-based conceptual framework used to decompact the core is insufficient here (Brain et al., 2011) because it does not account for post-depositional changes in compressibility. The modern analogue approach we have employed to assign compression properties downcore is not entirely valid in this case since we see a greater degree of compaction in some parts of the core than we would expect based on the compressibility of contemporary sediments. It is possible that parts of the core have been post-depositionally softened relative to the present-day salt-marsh sediments forming at East River Marsh.

Proxy reconstructions indicate that North America experienced two pre-industrial phases of climatic variability: the Medieval Climatic Anomaly (MCA; ~800 – 1300 CE) and the Little Ice Age (LIA; ~1400 – 1850 CE) (Mann et al., 2008; Pages 2k, 2013). In the northeastern and eastern central United States and relative to pre-industrial climate in the region, the MCA was characterized by warmer, drier conditions, persistent drought and increased catchment erosion, while the LIA was characterized by cooler and wetter conditions (Cook et al., 2004; Cronin et al., 2010; Cronin and Vann, 2003; Pederson et al., 2005; Peteet et al., 2007; Sritrairat et al., 2012). We note, however, that the MCA was not warmer than the present-day in North America (Pages 2k, 2013).

Values of PDL_{field} become positive and deviate from values of PDL_{model} at the onset of the MCA (~800 CE; Fig. 7 D). On this basis, we postulate that the MCA climate increased the susceptibility of salt-marsh sediments at East River Marsh to compaction between ~800 and 1300 CE by reducing the compressive yield stress of the sediments (Fig. 3 B) that formed during this period, such that they were more prone to compression at the low effective compressive stresses achievable in shallow intertidal stratigraphies. This weakening of MCA salt-marsh sediments would have made them vulnerable to future loading by overburden sediments (cf. DeLaune et al., 1994). The effect of this enhanced compaction of MCA sediments persists (within error) until the present day, as evidenced by positive values for PDL_{field} until at least 1800 CE (Fig. 7 D).

6.3 Modelling compaction and post-depositional lowering with reduced yield stresses

To assess whether this reduction in compressive yield strength is sufficient to explain the observed differences between trench and core RSL reconstructions at East River Marsh, we modified the Brain et al. (2011; 2012) compression-only model to quantitatively address our hypothesis that MCA warmth resulted in weakening of MCA sediments. Accordingly, we reduced the yield stress of core sediment that formed during the MCA by 90%, which we consider to be a feasible reduction based on contemporary observations of weakening of salt-marsh substrates due to biodegradation and bioturbation processes (Wilson et al., 2012) . This was achieved by specifying a continuous triangular probability distribution for σ'_y with a modal

value of 0.4 kPa and range of 0.35 – 0.84 kPa for layers between 134 cm and 98 cm that correspond to 800-1300 CE (Figs. 4 and 6). The yield stress distribution in all other layers was the same as that specified in Section 5. PDL predicted by this revised model (termed PDL_{bio}) is, within error, equal to PDL_{model} at 238-134 cm in the East River Marsh core (Fig. 4 D). Above 134 cm, PDL_{bio} is greater than PDL_{model} (by up to 7 cm at ~100 cm, or1300 CE) and notably, this effect of reducing yield stress only during the MCA (800-1300 CE) persists in the PDL profile until ~2000 CE. Bulk density predicted by the biodegradation-weakened model is comparable to those of the original, compression-only model (Figs. 4 and 10). Comparison of measured bulk density with those predicted by the biodegradation-weakened model yields a strong ($r^2_{adj} = 0.79$), positive and statistically-significant relationship ($p <0.0001$; Fig. 10 B).

Although PDL_{bio} is systematically lower than PDL_{field} these quantities are indistinguishable from one another within their uncertainties except for a difference of ~1.5 cm at ~1400-1600 CE (Fig. 7 D). Decompacting the core using PDL_{bio} results in no statistically-significant difference between the core and trench RSL reconstructions (Figs. 7 E). There is also an improved degree of similarity (compared to using PDL_{model} values) between the decompacted core and trench records based on comparison of modeled rates of RSL change and the timing of change points (Fig. 8; Table 3). Based on this improved fit between the core and PDL_{bio}-corrected core reconstructions, we deem both the proposed mechanism and magnitude of compressive strength reduction during the MCA to be feasible.

6.4 Causal processes and mechanisms

The exact mechanism for the postulated softening remains enigmatic and could result from the effects of multiple, yet currently poorly constrained, syn- and post-depositional processes. These are likely to be complex, interrelated and not purely a function of higher temperature during the MCA, since this is not warmer than those currently experienced in New England (Mann et al., 2008; Pages 2k, 2013) and contemporary salt-marsh sediments are seemingly less, not more, compressible than those that formed in the MCA. One possible explanation of the difference in sediment compressibility in the MCA and post-industrial warm episodes may relate to the physiological response of salt-marsh vegetation to atmospheric CO_2 concentrations, which are

higher today than during the MCA (Ahn et al., 2012; MacFarling Meure et al., 2006; Siegenthaler et al., 2005). Differences in CO_2 concentration can, in synergy with differences in temperature, salinity and nutrient status, drive differences in above- and below-ground productivity and the proportion of lignin production and the succulence and turgidity of plants (Couto et al., 2014; Deegan et al., 2012; Duarte et al., 2014). In turn, this can affect sediment compressibility because a reduction in the density, strength and depth of belowground roots and rhizomes can lower the compressive strength of the sediment (manifest as a reduction in yield stress) and render it more prone to compression and structural collapse (Brain et al., 2011; DeLaune et al., 1994; Schultz et al., 2016). However, whilst such experimental and modelling work on physiological responses to climate change is intriguing, links to compressibility are speculative and further work is required to determine how this varies in different climatic settings and for different salt-marsh plants.

Increased nutrient availability caused by greater catchment erosion and/or offshore primary productivity during the MCA may have reduced the need for salt-marsh plants to develop dense sub-surface root networks (Deegan et al., 2012), though again we would expect this, and its effect on compressibility, to be evident in our modern analogue samples given contemporary coastal eutrophication (Deegan et al., 2012).

Warmer temperatures during the MCA, in conjunction with a lower groundwater table at low tide that may have resulted from drier conditions, may have permitted greater opportunity for biodegradation-induced softening of near-surface organic matter. However, we see no obvious visual stratigraphic signature of bulk biodegradation during the MCA, though we note that this may be evident through more detailed geochemical investigation (Marshall et al., 2015; Slowakiewicz et al., 2015; Vane et al., 2001).

We do not consider the elevated temperatures of the MCA to have caused significant desiccation of the near-surface sediments because the salt marsh is diurnally flooded, though we note that the groundwater table at low tide may have been lower during the MCA that than during wetter periods (Brain et al., 2011). It is therefore possible that the effects of different vadose zone conditions during the MCA may have been most pronounced in the most aerated areas

surrounding belowground plant material, such as roots and rhizomes (Aitken et al., 2004; Atlas, 1981; Beazley et al., 2012; Cundy and Croudace, 1995; Oka et al., 2011; Osafune et al., 2014; Sánchez et al., 1998; Stumm and Morgan, 1995; van Huissteden and van de Plassche, 1998). This may also not be evident in the preserved lithostratigraphy in the core sediments, but degradation of structural plant material may explain the hypothesised softening.

Crabs such as *Uca pugnax* and *Sesarma reticulatum* can cause biodegradation by excavating and maintaining below-ground burrows in salt-marsh sediments (Katz, 1980; Schultz et al., 2016). These burrow structures reduce bulk density, while increasing net permeability and drainage, reduction-oxidation potential and decomposition rates of belowground salt-marsh vegetation (Bertness, 1985; Wilson et al., 2012). Contemporary studies that consider the effects of bioturbation on the geotechnical properties of salt-marsh have demonstrated that reduction in sediment shear strength of $\leq 90\%$ can occur as a result of reduced density and structural integrity of sub-surface biomass (roots and rhizomes) (Wilson et al., 2012). However, we discount any significant influence of bioturbation on the compressive strength of salt-marsh sediments on the basis that the core and trench stratigraphy do not display litho-, bio- or chemo-stratigraphic evidence of vertical mixing from macrofaunal burrowing activity (Figs. 2, 4, 5, 6). We also note that bioturbation by crab activity occurs primarily in the contemporary low salt-marsh environments (see section 2) that are not represented in our core of high salt-marsh sediment.

During the LIA, we do not consider reductions in the compressive strength of salt-marsh sediments to be likely. Cooler temperatures limit biodegradation and nutrient inputs, driven by reduced catchment and offshore primary productivity. Reduced nutrient inputs force salt-marsh plants to seek buried nutrient sources *via* dense root networks (Deegan et al., 2012). Consequently, we contend that significant syn-depositional changes to compressive strength did not occur within the LIA sediments at East River Marsh. We also do not consider the potential enhanced ice loading of the marsh surface during the LIA to be the cause of the observed offset between PDL_{feld} and PDL_{model}. Loading of the marsh surface by sea ice would, if effective, affect all sections of the core (i.e. not solely those that formed in the MCA). In addition, Argow and FitzGerald (2006) demonstrated that salt-marsh response to ice loading is elastic, with no permanent compaction following ice removal/melting.

38

6.5 Significance, implications and future work

We have demonstrated that approximately 75 - 90% of the maximum PDL observed at East River Marsh can be explained by increased compressibility of MCA sediments. This causes PDL that is nearly an order of magnitude greater than that experienced as a result of mechanical compression alone. At locations where salt-marsh environments are highly organic and in cores that span distinctive climate intervals, compression-only geotechnical models (Brain et al., 2015; Brain et al., 2011; Brain et al., 2012; Paul and Barras, 1998; Pizzuto and Schwendt, 1997) may not account for the principal cause of compaction and subsequently underestimate PDL. If we are to fully understand the drivers of sea level change, determining the mechanisms that control compressibility during the MCA is an important research objective. Until we have identified the causal mechanism and determined whether it operates locally or more widely, it is premature to deem all Common Era core-based RSL reconstructions as significantly impacted by sediment compaction. Indeed, the softening mechanism operating at East River Marsh may well be a local phenomenon that results from processes and conditions specific to the broad physiographic setting of Long Island Sound.

Since climate exerts a strong control on the specific processes of biodegradation, the effect on compaction and PDL is likely to be spatially and temporally variable. Some salt-marsh records may be unaffected by subtle climatic shifts because they do not result in ecological and/or (bio-) geomorphic thresholds being exceeded (cf. Deegan et al., 2012; Johnson, 2014; Long et al., 2006; Peteet, 2000; Sanford et al., 2006; Spencer et al., 1998). It is now necessary to identify where such sensitivity exists and to undertake further research into the controls on sediment compaction in organogenic salt-marsh stratigraphies to permit development of new geotechnical models that explicitly incorporate biodegradation processes. A primary challenge for this research is obtaining objective estimates of how the geotechnical properties of salt-marsh sediment in a single core varied through time in response to regional climate trends where there is not a compaction-free RSL reconstruction (e.g. the trench) available. This could be explored by generating new training sets of geotechnical data from modern salt-marsh sediments that span a range of climate zones and incorporate variability of dominant plant types and salt-marsh morphologies.

We note two broader implications of our findings. Firstly, our results reinforce the need to use unbroken sequences of high salt-marsh peat, supported wherever possible by compaction-free basal samples, to minimize the effects of compaction on RSL reconstructions in order to limit the contribution of denser layers to compaction of underlying material (Brain et al., 2015; Brain et al., 2012; Horton and Shennan, 2009; Long et al., 2006). We reiterate that the core analyzed here is not ideal for reconstructing RSL because it contains a subtly more minerogenic high salt-marsh stratum (Fig. 4 E) that may have contributed to enhanced compaction in the softened MCA sediments. In addition, use of high-marsh sediments only also removes the need to consider the space- and time-variable effects of bioturbation on compressive strength observed in the lower marsh environments favored by salt-marsh macrofauna. Secondly, the use of geotechnical models to project changes in salt-marsh surface elevation may underestimate the magnitude of compaction-induced surface lowering. Hence, model-based assessments of the fate of coastal wetlands in response to RSL rise may be overly optimistic and underestimate the rate of surface lowering through compaction if biodegradation and past climate changes are not considered (Kirwan et al., 2010; Kirwan et al., 2016; Mudd et al., 2009).

7. Conclusions

We produced a new RSL reconstruction from a sediment core collected at East River Marsh, Connecticut, USA. This reconstruction, which spans the period ~100 to 2000 CE, was considered to be prone to compaction-induced post-depositional lowering of samples within the core. We compared this core RSL reconstruction to a previously-published RSL reconstruction obtained from compaction-free basal sediments at East River Marsh and noted a statistically-significant difference in reconstructions between ~1100-1800 CE. The observed differences between the records can feasibly only be attributed to sediment compaction of the core. Through use of a geotechnical model, we demonstrated that mechanical compression alone cannot explain the observed offset between the core and trench RSL reconstructions. We hypothesised that the warmer, drier conditions experienced during the Medieval Climate Anomaly (MCA) resulted in a marked response in ecological and biogeochemical conditions at East River Marsh, which in turn reduced the compressive strength of sediment that formed during the MCA. The effect of this weakening on post-depositional lowering of overlying sediment persists to the present day. Through numerical simulation of biodegradation-induced weakening of MCA sediments in the core, the accuracy of our compaction model improved greatly, accounting for the offset between records and increasing confidence in the validity of our proposed weakening mechanism.

Geotechnical modelling alone may be insufficient to accurately decompact salt-marsh sediments and/or project surface elevation changes in coastal wetlands in locations that are ecologically and geomorphologically sensitive to climatic fluctuations. In turn, this may result in a misinterpretation of historic RSL changes and causal mechanisms and an overly-optimistic outlook on coastal wetland survival. Our work reinforces the need to use continuous successions of highly-organic, low-density high-marsh peats to reconstruct Common Era RSL, as has been undertaken elsewhere along the North American Atlantic coast and elsewhere. We advocate further research into the controls and effects of climatic and ecological processes on the geotechnical properties of organogenic salt-marsh sediments to improve the predictive capacity of compaction models.

Acknowledgements

References

Ahn, J., Brook, E.J., Mitchell, L., Rosen, J., McConnell, J.R., Taylor, K., Etheridge, D., Rubino, M., 2012. Atmospheric CO2 over the last 1000 years: A high-resolution record from the West Antarctic Ice Sheet (WAIS) Divide ice core. Global Biogeochemical Cycles 26, n/a-n/a.

Aitken, C.M., Jones, D.M., Larter, S.R., 2004. Anaerobic hydrocarbon biodegradation in deep subsurface oil reservoirs. Nature 431, 291-294.

Allen, J.R.L., 1999. Geological impacts on coastal wetland landscapes: some general effects of sediment autocompaction in the Holocene of northwest Europe. The Holocene 9, 1-12.

Allen, J.R.L., 2000. Morphodynamics of Holocene salt marshes: a review sketch from the Atlantic and Southern North Sea coasts of Europe. Quaternary Science Reviews 19, 1155-1231.

Argow, B.A., FitzGerald, D.M., 2006. Winter processes on northern salt marshes: Evaluating the impact of in-situ peat compaction due to ice loading, Wells, ME. Estuarine, Coastal and Shelf Science 69, 360-369.

Atlas, R.M., 1981. Microbial degradation of petroleum hydrocarbons: an environmental perspective. Microbiological Reviews 45, 180-209.

Beazley, M.J., Martinez, R.J., Rajan, S., Powell, J., Piceno, Y.M., Tom, L.M., Andersen, G.L., Hazen, T.C., Van Nostrand, J.D., Zhou, J., Mortazavi, B., Sobecky, P.A., 2012. Microbial Community Analysis of a Coastal Salt Marsh Affected by the *Deepwater Horizon* Oil Spill. PLoS ONE 7, e41305.

Bertness, M.D., 1985. Fiddler Crab Regulation of Spartina alterniflora Production on a New England Salt Marsh. Ecology 66, 1042-1055.

Bertness, M.D., Miller, T., 1984. The distribution and dynamics of Uca pugnax (Smith) burrows in a new England salt marsh. Journal of Experimental Marine Biology and Ecology 83, 211-237.

Bloom, A.L., 1964. Peat accumulation and compaction in Connecticut coastal marsh. Journal of Sedimentary Research 34, 599-603.

Boyle, J., 2004. A comparison of two methods for estimating the organic matter content of sediments. Journal of Paleolimnology 31, 125-127.

Brain, M.J., 2015. Compaction, Handbook of Sea-Level Research. John Wiley & Sons, Ltd, pp. 452-469.

Brain, M.J., Kemp, A.C., Horton, B.P., Culver, S.J., Parnell, A.C., Cahill, N., 2015. Quantifying the contribution of sediment compaction to late Holocene salt-marsh sea-level reconstructions, North Carolina, USA. Quaternary Research 83, 41-51.

Brain, M.J., Long, A.J., Petley, D.N., Horton, B.P., Allison, R.J., 2011. Compression behaviour of minerogenic low energy intertidal sediments. Sedimentary Geology 233, 28-41.

Brain, M.J., Long, A.J., Woodroffe, S.A., Petley, D.N., Milledge, D.G., Parnell, A.C., 2012. Modelling the effects of sediment compaction on salt marsh reconstructions of recent sea-level rise. Earth and Planetary Science Letters 345-348, 180-193.

Cahill, N., Kemp, A.C., Horton, B.P., Parnell, A.C., 2015a. Modeling sea-level change using errors-in-variables integrated Gaussian processes. 547-571.

Cahill, N., Rahmstorf, S., Parnell, A.C., 2015b. Change points of global temperature. Environmental Research Letters 10, 084002.

Carlin, B.P., Gelfand, A.E., Smith, A.F.M., 1992. Hierarchical Bayesian Analysis of Changepoint Problems. Applied Statistics 41, 389-405.

Cook, E.R., Woodhouse, C.A., Eakin, C.M., Meko, D.M., Stahle, D.W., 2004. Long-Term Aridity Changes in the Western United States. Science 306, 1015-1018.

Couto, T., Martins, I., Duarte, B., Cacador, I., 2014. Modelling the effects of global temperature increase on the growth of salt marsh plants. Applied Ecology and Environmental Research 12, 753-764.

Craft, C.B., Seneca, E.D., Broome, S.W., 1993. Vertical Accretion in Microtidal Regularly and Irregularly Flooded Estuarine Marshes. Estuarine, Coastal and Shelf Science 37, 371-386.

Cronin, T.M., Hayo, K., Thunell, R.C., Dwyer, G.S., Saenger, C., Willard, D.A., 2010. The Medieval Climate Anomaly and Little Ice Age in Chesapeake Bay and the North Atlantic Ocean. Palaeogeography, Palaeoclimatology, Palaeoecology 297, 299-310.

Cronin, T.M., Vann, C.D., 2003. The sedimentary record of climatic and anthropogenic influence on the Patuxent estuary and Chesapeake Bay ecosystems. Estuaries 26, 196-209.

Crooks, S., 1999. A mechanism for the formation of overconsolidated horizons within estuarine floodplain alluvium: implications for the interpretation of Holocene sea-level curves. Geological Society, London, Special Publications 163, 197-215.

Cundy, A.B., Croudace, I.W., 1995. Sedimentary and geochemical variations in a salt marsh/mud flat environment from the mesotidal Hamble estuary, southern England. Marine Chemistry 51, 115-132.

Deegan, L.A., Johnson, D.S., Warren, R.S., Peterson, B.J., Fleeger, J.W., Fagherazzi, S., Wollheim, W.M., 2012. Coastal eutrophication as a driver of salt marsh loss. Nature 490, 388-392.

DeLaune, R.D., Nyman, J.A., Patrick, W.H., 1994. Peat collapse, ponding, and wetland loss in a rapidly submerging coastal marsh. Journal of Coastal Research 10, 1021-1030.

Duarte, B., Santos, D., Silva, H., Marques, J.C., Caçador, I., 2014. Photochemical and biophysical feedbacks of C3 and C4 Mediterranean halophytes to atmospheric CO_2 enrichment confirmed by their stable isotope signatures. Plant Physiology and Biochemistry 80, 10-22.

Dutton, A., Carlson, A.E., Long, A.J., Milne, G.A., Clark, P.U., DeConto, R., Horton, B.P., Rahmstorf, S., Raymo, M.E., 2015. Sea-level rise due to polar ice-sheet mass loss during past warm periods. Science 349.

Edwards, R.J., Wright, A.J., van de Plassche, O., 2004. Surface distributions of salt-marsh foraminifera from Connecticut, USA: modern analogues for high-resolution sea level studies. Marine Micropaleontology 51, 1-21.

Gabet, E.J., 1998. Lateral migration and bank erosion in a saltmarsh tidal channel in San Francisco Bay, California. Estuaries 21, 745-753.

Gehrels, W.R., 1994. Determining relative sea-level change from salt-marsh foraminifera and plant zones on the coast of Maine, U.S.A. Journal of Coastal Research 10, 990-1009.

Gehrels, W.R., 2000. Using foraminiferal transfer functions to produce high-resolution sea-level records from salt-marsh deposits, Maine, USA. The Holocene 10, 367-376.

Gehrels, W.R., Callard, S.L., Moss, P.T., Marshall, W.A., Blaauw, M., Hunter, J., Milton, J.A., Garnett, M.H., 2012. Nineteenth and twentieth century sea-level changes in Tasmania and New Zealand. Earth and Planetary Science Letters 315–316, 94-102.

Gehrels, W.R., van de Plassche, O., 1999. The use of *Jadammina macrescens* (Brady) and *Balticammina pseudomacrescens* Brönnimann, Lutze and Whittaker (Protozoa: Foraminiferida) as sea-level indicators. Palaeogeography, Palaeoclimatology, Palaeoecology 149, 89-101.

Greensmith, J.T., Tucker, M.V., 1971. Overconsolidation in some fine-grained sediments, its nature, genesis and value in interpreting the history of certain English Quaternary deposits. Geologie en Mijnbouw 50, 743-748.

Grimm, E.C., 1987. CONISS: a FORTRAN 77 program for stratigraphically constrained cluster analysis by the method of incremental sum of squares. Computers & Geosciences 13, 13-35.

Hales, T.C., Ford, C.R., Hwang, T., Vose, J.M., Band, L.E., 2009. Topographic and ecologic controls on root reinforcement. Journal of Geophysical Research: Earth Surface 114, n/a-n/a.

Haslett, J., Parnell, A., 2008. A simple monotone process with application to radiocarbon-dated depth chronologies. Journal of the Royal Statistical Society: Series C (Applied Statistics) 57, 399-418.

Hawkins, A.B., 1984. Depositional characteristics of estuarine alluvium: some engineering implications. Quarterly Journal of Engineering Geology and Hydrogeology 17, 219-234.

Head, K.H., 2008. Manual of Soil Laboratory Testing Volume II: Soil Classification and Compaction Tests. Whittles, Caithness.

Head, K.H., Epps, R.J., 2011. Manual of Soil Laboratory Testing Volume II: Permeability, Shear Strength and Compressibility Tests. Whittles, Caithness.

Heiri, O., Lotter, A.F., Lemcke, G., 2001. Loss on ignition as a method for estimating organic and carbonate content in sediments: reproducibility and comparability of results. Journal of Paleolimnology 25, 101-110.

Hobbs, N.B., 1986. Mire morphology and the properties and behaviour of some British and foreign peats. Quarterly Journal of Engineering Geology and Hydrogeology 19, 7-80.

Horton, B.P., Edwards, R.J., 2006. Quantifying Holocene sea-level change using intertidal foraminifera: lessons from the British Isles. Cushman Foundation for Foraminiferal Research, Special Publication 40, 97.

Horton, B.P., Rahmstorf, S., Engelhart, S.E., Kemp, A.C., 2014. Expert assessment of sea-level rise by AD 2100 and AD 2300. Quaternary Science Reviews 84, 1-6.

Horton, B.P., Shennan, I., 2009. Compaction of Holocene strata and the implications for relative sealevel change on the east coast of England. Geology 37, 1083-1086.

Jackson, S.T., Williams, J.W., 2004. Modern analogs in Quaternary paleoecology: Here today, gone yesterday, gone tomorrow? Annual Review of Earth and Planetary Sciences 32, 495-537.

Johnson, D.S., 2014. Fiddler on the roof: a northern range extension for the marsh fiddler crab. Journal of Crustacean Biology 34, 671-673.

Juggins, S., 2013. rioja: Analysis of Quaternary Science Data, R package version (0.9-9). http://cran.r-project.org/package=rioja.

Juggins, S., Birks, H.J.B., 2012. Quantiative environmental reconstructions from biological data, in: Birks, H.J.B., Lotter, A.F., Juggins, S., Smol, J.P. (Eds.), Tracking environmental change using lake sediments: Data handling and numerical techniques. Springer, pp. 431-494.

Katz, L.C., 1980. Effects of burrowing by the fiddler crab, Uca pugnax (Smith). Estuarine and Coastal Marine Science 11, 233-237.

Kemp, A.C., Hawkes, A.D., Donnelly, J.P., Vane, C.H., Horton, B.P., Hill, T.D., Anisfeld, S.C., Parnell, A.C., Cahill, N., 2015a. Relative sea-level change in Connecticut (USA) during the last 2200 years. Earth and Planetary Science Letters 428, 217-229.

Kemp, A.C., Hawkes, A.D., Donnelly, J.P., Vane, C.H., Horton, B.P., Hill, T.D., Anisfeld, S.C., Parnell, A.C., Cahill, N., 2015b. Relative sea-level change in Connecticut (USA) during the last 2200 yrs. Earth and Planetary Science Letters 428, 217-229.

Kemp, A.C., Horton, B., Donnelly, J.P., Mann, M.E., Vermeer, M., Rahmstorf, S., 2011. Climate related sea-level variations over the past two millennia. Proceedings of the National Academy of Sciences 108, 11017-11022.

Kemp, A.C., Horton, B.P., Culver, S.J., Corbett, D.R., van de Plassche, O., Gehrels, W.R., Douglas, B.C., Parnell, A.C., 2009. Timing and magnitude of recent accelerated sea-level rise (North Carolina, United States). Geology 37, 1035-1038.

Kemp, A.C., Horton, B.P., Vane, C.H., Corbett, D.R., Bernhardt, C.E., Engelhart, S.E., Anisfeld, S.C., Parnell, A.C., Cahill, N., 2013. Sea-level change during the last 2500 years in New Jersey, USA. Quaternary Science Reviews 81, 90-104.

Kemp, A.C., Horton, B.P., Vann, D.R., Engelhart, S.E., Vane, C.H., Nikitina, D., Anisfeld, S.C., 2012. Quantitative vertical zonation of salt-marsh foraminifera for reconstructing former sea level; an example from New Jersey, USA. Quaternary Science Reviews 54, 26-39.

Khan, N.S., Ashe, E., Shaw, T.A., Vacchi, M., Walker, J., Peltier, W.R., Kopp, R.E., Horton, B.P., 2015. Holocene Relative Sea-Level Changes from Near-, Intermediate-, and Far-Field Locations. Current Climate Change Reports 1, 247-262.

Kirwan, M.L., Guntenspergen, G.R., D'Alpaos, A., Morris, J.T., Mudd, S.M., Temmerman, S., 2010. Limits on the adaptability of coastal marshes to rising sea level. Geophysical Research Letters 37.

Kirwan, M.L., Temmerman, S., Skeehan, E.E., Guntenspergen, G.R., Fagherazzi, S., 2016. Overestimation of marsh vulnerability to sea level rise. Nature Clim. Change 6, 253-260.

Kopp, R.E., Kemp, A.C., Bittermann, K., Horton, B.P., Donnelly, J.P., Gehrels, W.R., Hay, C.C., Mitrovica, J.X., Morrow, E.D., Rahmstorf, S., 2016. Temperature-driven global sea-level variability in the Common Era. Proceedings of the National Academy of Sciences 113, E1434-E1441.

Lillebø, A.I., Flindt, M.R., Pardal, M.Â., Marques, J.C., 1999. The effect of macrofauna, meiofauna and microfauna on the degradation of Spartina maritima detritus from a salt marsh area. Acta Oecologica 20, 249-258.

Long, A.J., Waller, M.P., Stupples, P., 2006. Driving mechanisms of coastal change: Peat compaction and the destruction of late Holocene coastal wetlands. Marine Geology 225, 63-84.

MacFarling Meure, C., Etheridge, D., Trudinger, C., Steele, P., Langenfelds, R., van Ommen, T., Smith, A., Elkins, J., 2006. Law Dome CO2, CH4 and N2O ice core records extended to 2000 years BP. Geophysical Research Letters 33, n/a-n/a.

Mann, M.E., Zhang, Z., Hughes, M.K., Bradley, R.S., Miller, S.K., Rutherford, S., Ni, F., 2008. Proxy-based reconstructions of hemispheric and global surface temperature variations over the past two millennia. Proceedings of the National Academy of Sciences 105, 13252-13257.

Marshall, C., Uguna, J., Large, D.J., Meredith, W., Jochmann, M., Friis, B., Vane, C.H., Spiro, B.F., Snape, C.E., Orheim, A., 2015. Geochemistry and petrology of palaeocene coals from Spitzbergen — Part 2: Maturity variations and implications for local and regional burial models. International Journal of Coal Geology 143, 1-10.

Morris, J.T., Sundareshwar, P.V., Nietch, C.T., Kjerfve, B., Cahoon, D.R., 2002. Response of coastal wetlands to rising sea level. Ecology 83, 2869-2877.

Mudd, S.M., Howell, S.M., Morris, J.T., 2009. Impact of dynamic feedbacks between sedimentation, sea-level rise, and biomass production on near-surface marsh stratigraphy and carbon accumulation. Estuarine, Coastal and Shelf Science 82, 377-389.

Niering, W.A., Warren, R.S., 1980. Vegetation Patterns and Processes in New England Salt Marshes. BioScience 30, 301-307.

Nydick, K.R., Bidwell, A.B., Thomas, E., Varekamp, J.C., 1995. Coastal Evolution in the Quarternary: IGCP Project 274A sea-level rise curve from Guilford, Connecticut, USA. Marine Geology 124, 137-159.

Oka, A.R., Phelps, C.D., Zhu, X., Saber, D.L., Young, L.Y., 2011. Dual Biomarkers of Anaerobic Hydrocarbon Degradation in Historically Contaminated Groundwater. Environmental Science & Technology 45, 3407-3414.

Orson, R.A., Warren, R.S., Niering, W.A., 1987. Development of a tidal marsh in a New England river valley. Estuaries 10, 20-27.

Osafune, S., Masuda, S., Sugiura, N., 2014. Role of the oceanic bridge in linking the 18.6 year modulation of tidal mixing and long-term SST change in the North Pacific. Geophysical Research Letters 41, 7284-7290.

Pages 2k, C., 2013. Continental-scale temperature variability during the past two millennia. Nature Geoscience 6, 339-346.

Parnell, A.C., Haslett, J., Allen, J.R.M., Buck, C.E., Huntley, B., 2008. A flexible approach to assessing synchroneity of past events using Bayesian reconstructions of sedimentation history. Quaternary Science Reviews 27, 1872-1885.

Paul, M.A., Barras, B.F., 1998. A geotechnical correction for post-depositional sediment compression" examples from the Forth valley, Scotland. Journal of Quaternary Science 13, 171-176.

Pederson, D.C., Peteet, D.M., Kurdyla, D., Guilderson, T., 2005. Medieval Warming, Little Ice Age, and European impact on the environment during the last millennium in the lower Hudson Valley, New York, USA. Quaternary Research 63, 238-249.

Peteet, D., 2000. Sensitivity and rapidity of vegetational response to abrupt climate change. Proceedings of the National Academy of Sciences 97, 1359-1361.

Peteet, D.M., Pederson, D.C., Kurdyla, D., Guilderson, T., 2007. Hudson River paleoecology from marshes: Environmental change and its implications for fisheries., in: J.R. Waldman, K.E.L., and D. Strayer, (Ed.), Hudson River Fishes and Their Environment, A.F.S. Symposium 51. American Fisheries Society, pp. 112-128.

Pizzuto, J.E., Schwendt, A.E., 1997. Mathematical modeling of autocompaction of a Holocene transgresive valley-fill deposit, Wolfe Glade, Delaware. Geology 25, 57-60.

Plater, A.J., Kirby, J.R., Boyle, J.F., Shaw, T., Mills, H., 2015. Loss on ignition and organic content, Handbook of Sea-Level Research. John Wiley & Sons, Ltd, pp. 312-330.

Powrie, W., 2014. Soil Mechanics: Concepts and Applications. CRC Press/Taylor and Francis, Baton Rouge.

PRISM, 2004. PRISM Climate Group, Oregon State University, http://prism.oregonstate.edu, created 4 Feb 2004. Accessed 26 July 2016.

Redfield, A.C., 1972. Development of a New England salt marsh. Ecological Monographs 42, 201-237.

Reimer, P.J., Bard, E., Bayliss, A., Beck, J.W., Blackwell, P.G., Bronk Ramsey, C., Grootes, P.M., Guilderson, T.P., Haflidason, H., Hajdas, I., Hatté, C., Heaton, T.J., Hoffmann, D.L., Hogg, A.G., Hughen, K.A., Kaiser, K.F., Kromer, B., Manning, S.W., Niu, M., Reimer, R.W., Richards, D.A., Scott, E.M., Southon, J.R., Staff, R.A., Turney, C.S.M., van der Plicht, J., 2013. IntCal13 and Marine13 Radiocarbon Age Calibration Curves 0–50,000 Years cal BP. Radiocarbon 55.

Rowley, D.B., Forte, A.M., Moucha, R., Mitrovica, J.X., Simmons, N.A., Grand, S.P., 2013. Dynamic Topography Change of the Eastern United States Since 3 Million Years Ago. Science 340, 1560-1563.

Saher, M.H., Gehrels, W.R., Barlow, N.L.M., Long, A.J., Haigh, I.D., Blaauw, M., 2015. Sea-level changes in Iceland and the influence of the North Atlantic Oscillation during the last half millennium. Quaternary Science Reviews 108, 23-36.

Sánchez, J.M., Otero, X.L., Izco, J., 1998. Relationships between vegetation and environmental characteristics in a salt-marsh system on the coast of Northwest Spain. Plant Ecology 136, 1-8.

Sanford, E., Holzman, S.B., Haney, R.A., Rand, D.M., Bertness, M.D., 2006. Larvel tolerance, gene flow, and the northern geographic range limit of fiddler crabs. Ecology 87, 2882-2894.

Schultz, R.A., Anisfeld, S.C., Hill, T.D., 2016. Submergence and Herbivory as Divergent Causes of Marsh Loss in Long Island Sound. Estuaries and Coasts, 1-9.

Scott, D.B., Medioli, F.S., 1978. Vertical zonations of marsh foraminifera as accurate indicators of former sea levels. Nature 272, 528-531.

Selby, M.J., 1993. Hillslope Materials and Processes. Oxford University Press, Oxford.

Siegenthaler, U.R.S., Monnin, E., Kawamura, K., Spahni, R., Schwander, J., Stauffer, B., Stocker, T.F., Barnola, J.-M., Fischer, H., 2005. Supporting evidence from the EPICA Dronning Maud Land ice core for atmospheric CO_2 changes during the past millennium. Tellus B 57, 51-57.

Simpson, G.L., 2012. Analogue methods, in: Birks, H.J.B., Lotter, A.F., Juggins, S., Smol, J.P. (Eds.), Data handling and numerical techniques. Springer, pp. 495-522.

Slowakiewicz, M., Tucker, M., Vane, C.H., Harding, R., Collins, A., Pancost, R.D., 2015. Shale-gas potential of the mid-Carboniferous Bowland-Hodder unit in the Cleveland basin (Yorkshire), Central Britain. Journal of Petroleum Geology 38, 1-18.

Sommerfield, C.K., 2006. On sediment accumulation rates and stratigraphic completeness: Lessons from Holocene ocean margins. Continental Shelf Research 26, 2225-2240.

Spencer, C.D., Plater, A.J., Long, A.J., 1998. Rapid coastal change during the mid- to late Holocene: the record of barrier estuary sedimentation in the Romney Marsh region, southeast England. The Holocene 8, 143-163.

Sritrairat, S., Peteet, D.M., Kenna, T.C., Sambrotto, R., Kurdyla, D., Guilderson, T., 2012. A history of vegetation, sediment and nutrient dynamics at Tivoli North Bay, Hudson Estuary, New York. Estuarine, Coastal and Shelf Science 102–103, 24-35.

Stumm, W., Morgan, J.J., 1995. Aquatic Chemistry: Chemical Equilibria and Rates in Natural Waters. Wiley Interscience, New York.

Tamisiea, M.E., 2011. Ongoing glacial isostatic contributions to observations of sea level change. Geophysical Journal International 186, 1036-1044.

van Asselen, S., Stouthamer, E., van Asch, T.W.J., 2009. Effects of peat compaction on delta evolution: A review on processes, responses, measuring and modeling. Earth-Science Reviews 92, 35-51.

Van Eerdt, M.M., 1985. Salt marsh cliff stability in the oosterschelde. Earth Surface Processes and Landforms 10, 95-106.

van Huissteden, J., van de Plassche, O., 1998. Sulphate reduction as a geomorphological agent in tidal marshes ('Great Marshes' at Barnstable, Cape Cod, USA). Earth Surface Processes and Landforms 23, 223-236.

Vane, C.H., Martin, S.C., Snape, C.E., Abbott, G.D., 2001. Degradation of lignin in wheat straw during growth of the oyster mushroom (Pleurotus ostreatus) using off-line thermochemolysis with tetramethylammonium hydroxide and solid- state C-13 NMR. Journal of Agricultural and Food Chemistry 49, 2709-2716.

Watcham, E.P., Shennan, I., Barlow, N.L.M., 2013. Scale considerations in using diatoms as indicators of sea-level change: lessons from Alaska. Journal of Quaternary Science 28, 165-179.

Wilson, C.A., Hughes, Z.J., FitzGerald, D.M., 2012. The effects of crab bioturbation on Mid-Atlantic saltmarsh tidal creek extension: Geotechnical and geochemical changes. Estuarine, Coastal and Shelf Science 106, 33-44.

Wright, A.J., Edwards, R.J., van de Plassche, O., 2011. Reassessing transfer-function performance in sea-level reconstruction based on benthic salt-marsh foraminifera from the Atlantic coast of NE North America. Marine Micropaleontology 81, 43-62.

Wright, A.J., Edwards, R.J., van de Plassche, O., Blaauw, M., Parnell, A.C., van der Borg, K., de Jong, A.F.M., Roe, H.M., Selby, K., Black, S., 2017. Reconstructing the accumulation history of a saltmarsh sediment core: Which age-depth model is best? Quaternary Geochronology 39, 35-67.